Supporting Information

Functional Biomimietics for Copper Oxidases: Interesting Catalytic Promiscuity of Novel Monocopper(II) Complexes

Vigneswara Chellam Ravisankar[a], Balasubramaniam Selvakumaran[a], Tamilarasan Ajaykamal[b] and Mariappan Murali[a]*,

[a]*Coordination and Bioinorganic Chemistry Research Laboratory, Department of Chemistry, National College (Autonomous) affiliated to Bharathidasan University, Tiruchirappalli 620 001, Tamil Nadu, India*
[b]*School of Chemistry, Bharathidasan University, Tiruchirappalli 620 024, Tamil Nadu, India*

*Corresponding author: Mariappan Murali: murali@nct.ac.in and ma66mu@gmail.com

Tel.: +91 97901 80077

fax: +91 431 2481997

Table of contents:

1. Computational protocol

The coordination geometries of copper(II) mixed ligand complexes in the ground state with doublet spin state were optimized by using density functional theory (DFT) at the B3LYP level of theory by employing the Gaussian 09 program package[1]. The calculations were administrated with a mixed basis set (B1) of LANL2DZ for the copper metal atom, which contains a relativistic effective core potential with a valence basis set and 6-31G* for the remaining atoms[2]. The normal mode analyses were performed to examine the minimal energy nature of the geometry. The copper(II) complexes **1** and **2** were considered as mono-positive cations as the copper metal was considered in +2 oxidation state and doublet spin state whereas the ligand H(mq) as a mono-negative ligand. The salvation of the complexes was applied by employing the CPCM method using methanol as the solvent.

Charge distribution and molecular orbital analyses

We used the natural bond orbital (NBO)[3] approach to calculate the atomic charge distribution on each complex atom. From the NBO analysis, we can predict electron delocalization, atomic charge distribution, and intra-atomic interaction of atoms within a compound.[3] The energies of the frontier molecular orbitals (FMOs),[4] the highest and second-highest occupied molecular orbitals (EHOMO and EHOMO−1) and the lowest and second-lowest unoccupied molecular orbitals (ELUMO and ELUMO+1), were calculated. Some quantum chemical descriptors including ionization potential (IP),[5] electron affinity (EA),[5] band gap (ΔE), chemical hardness (η),[6] global softness (S),[6] electrochemical potential (μ),[7]electrophilicity index (ω),[8] and electronegativity (χ)[7] were estimated as outlined in eqs 1-8.

$$\mathrm{IP} = -E_{\mathrm{HOMO}} \quad (1)$$

$$\mathrm{EA} = -E_{\mathrm{LUMO}} \quad (2)$$

$$\Delta E = E_{\mathrm{LUMO}} - E_{\mathrm{HOMO}} \quad (3)$$

$$\eta = \frac{E_{\mathrm{LUMO}} - E_{\mathrm{HOMO}}}{2} \quad (4)$$

$$S = 1/\eta \quad (5)$$

$$\mu = -\frac{\mathrm{IP} + \mathrm{EA}}{2} \quad (6)$$

$$\omega = \mu^2 \quad (7)$$

$$\chi = -\mu \sqrt{2\eta} \qquad (8)$$

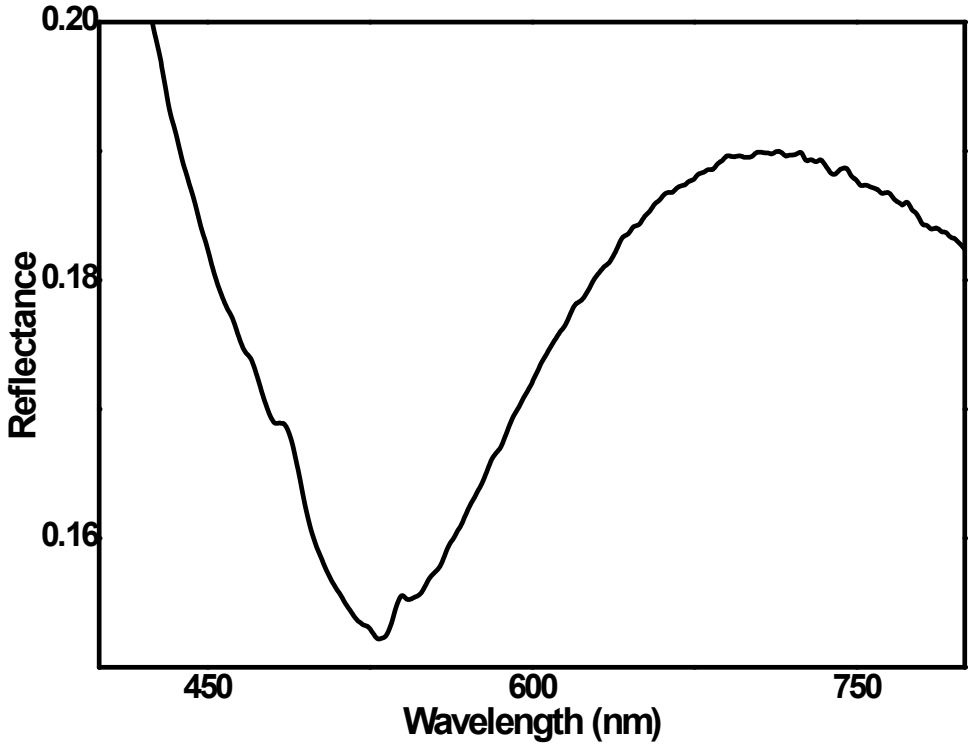

Fig. S1 Reflectance spectrum of $[Cu(L^1)(phen)](ClO_4)$ (**1**).

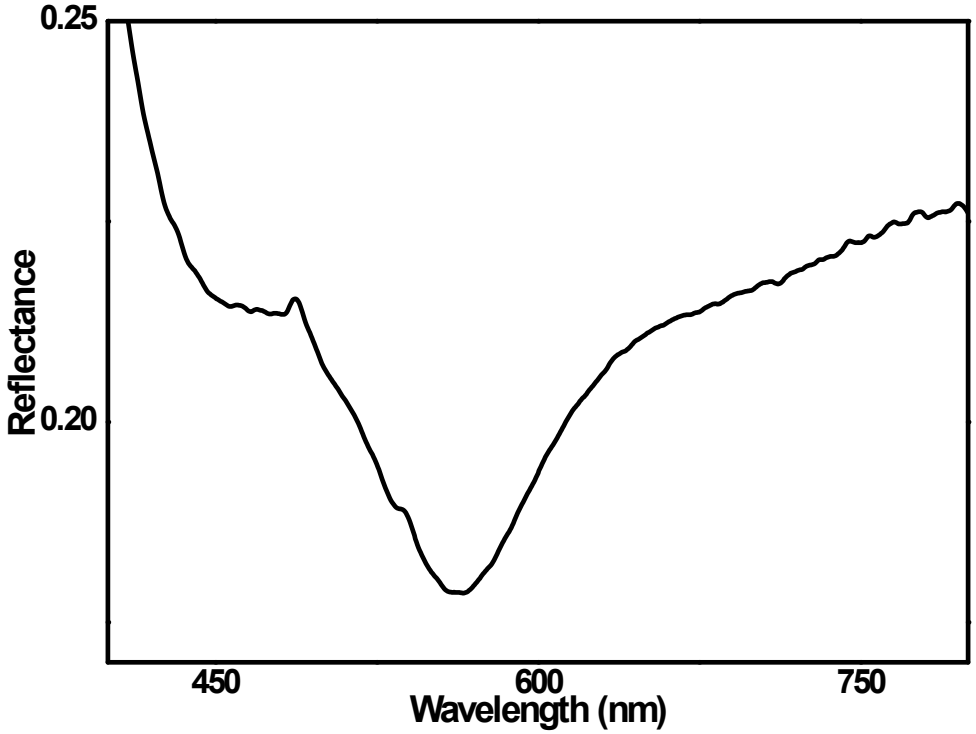

Fig. S2 Reflectance spectrum of $[Cu(L^2)(phen)](ClO_4)$ (**2**).

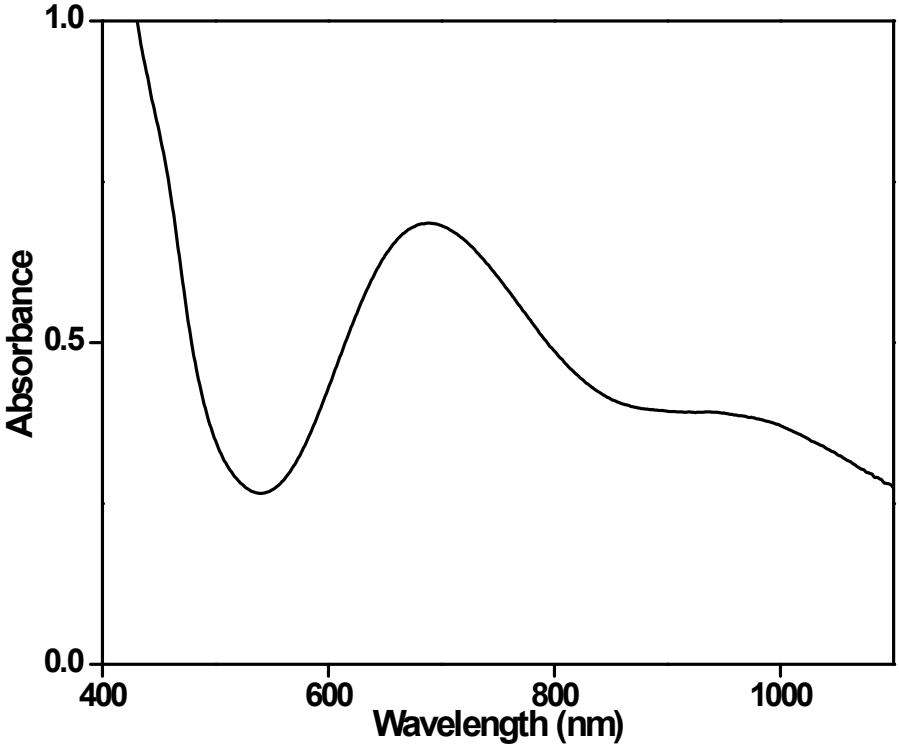

Fig. S3 Electronic spectrum of $[Cu(L^1)(phen)](ClO_4)$ (**1**) in MeOH.

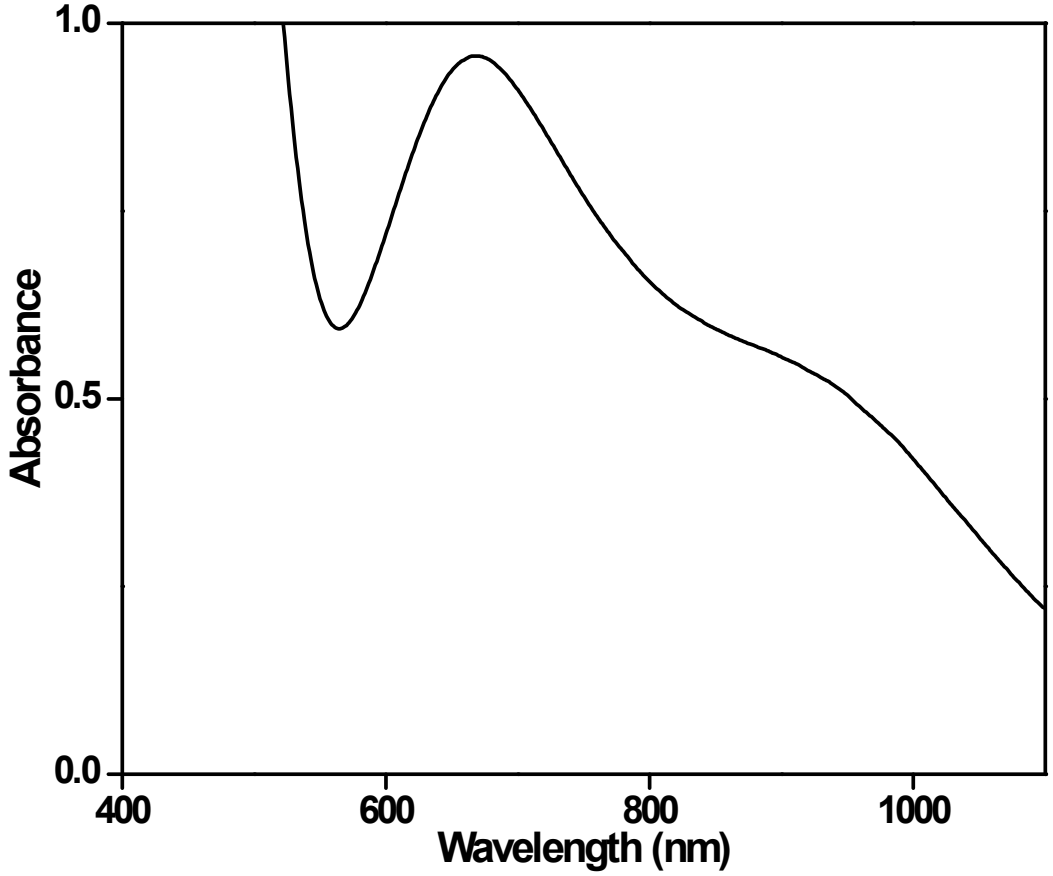

Fig. S4 Electronic spectrum of $[Cu(L^2)(phen)](ClO_4)$ (**2**) in MeOH.

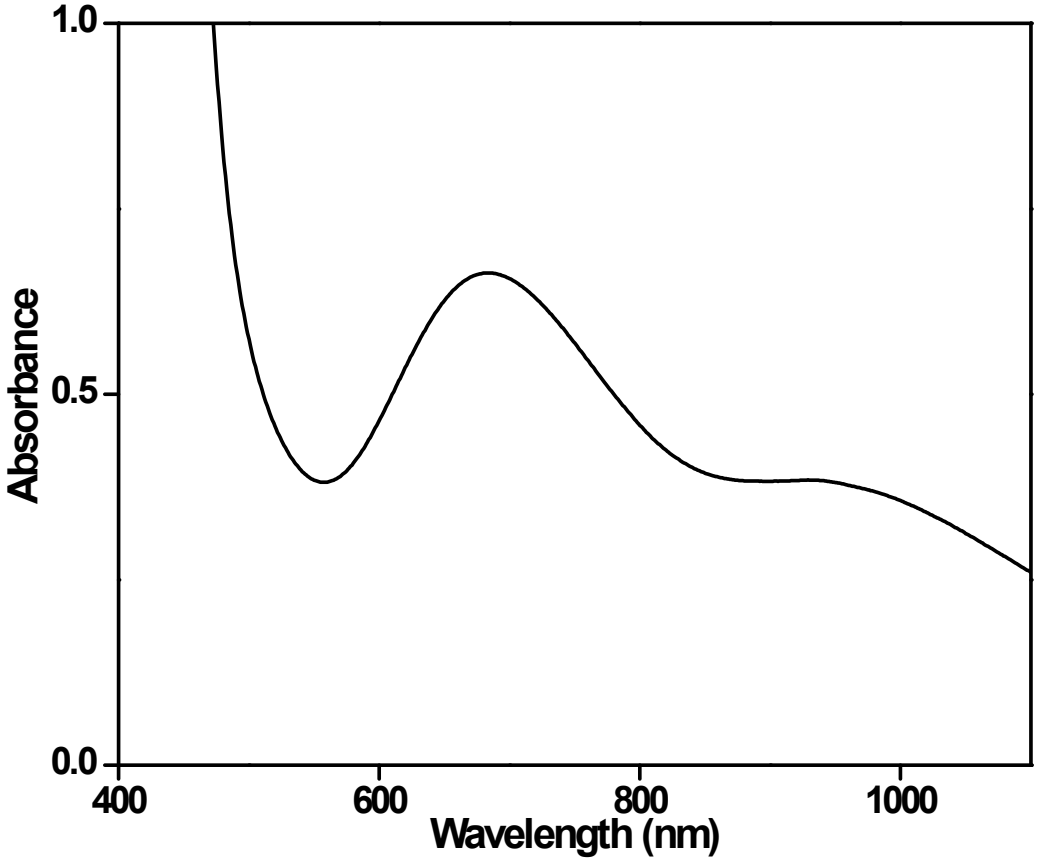

Fig. S5 Electronic spectrum of $[Cu(L^1)(phen)](ClO_4)$ (**1**) in MeOH:H_2O (4:1 v/v).

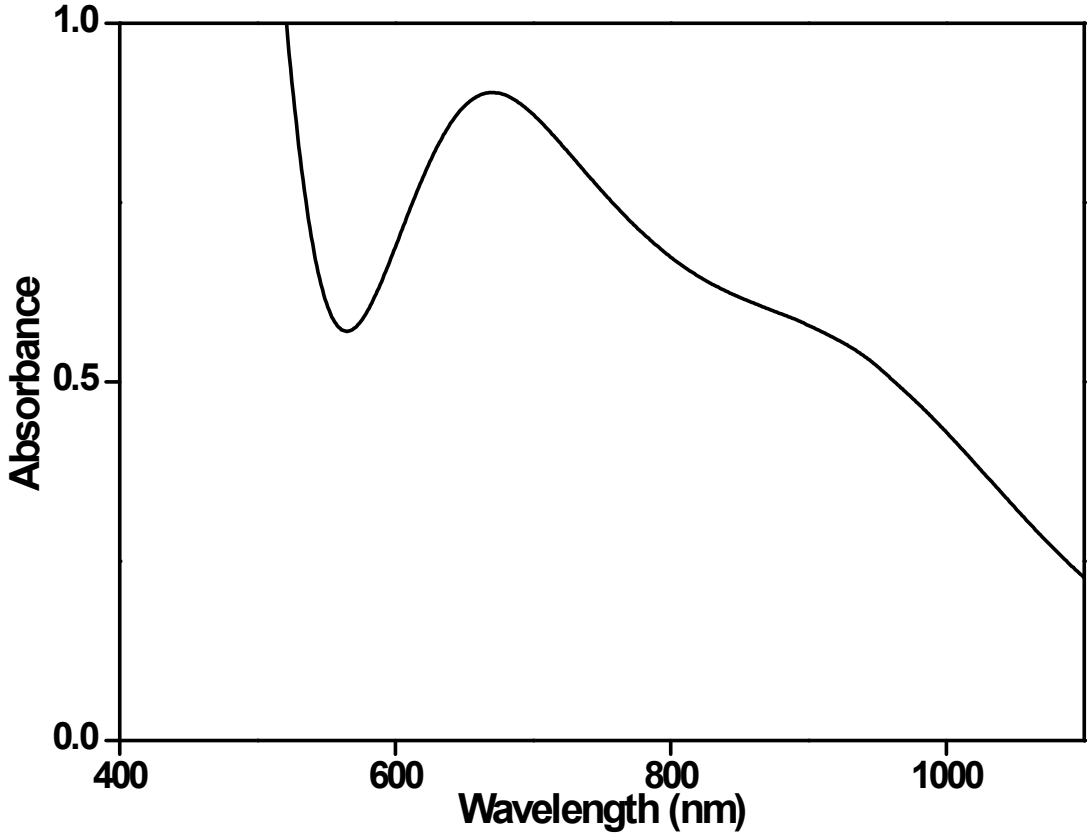

Fig. S6 Electronic spectrum of $[Cu(L^2)(phen)](ClO_4)$ (**2**) in MeOH:H_2O (4:1 v/v).

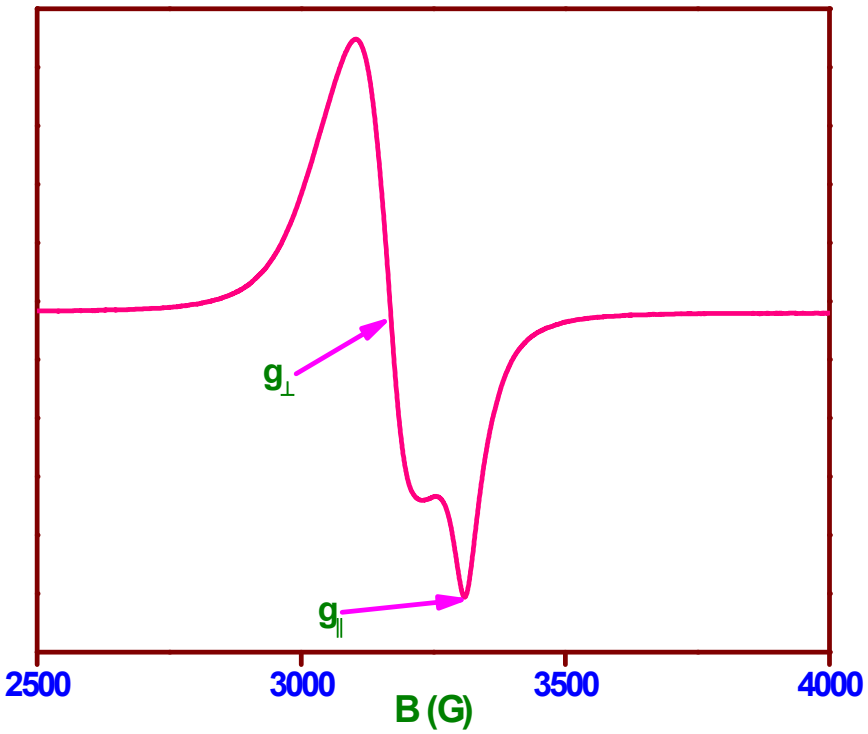

Fig. S7 Polycrystalline EPR spectra of [Cu(L^1)(phen)](ClO_4) (**1**) at room temperature.

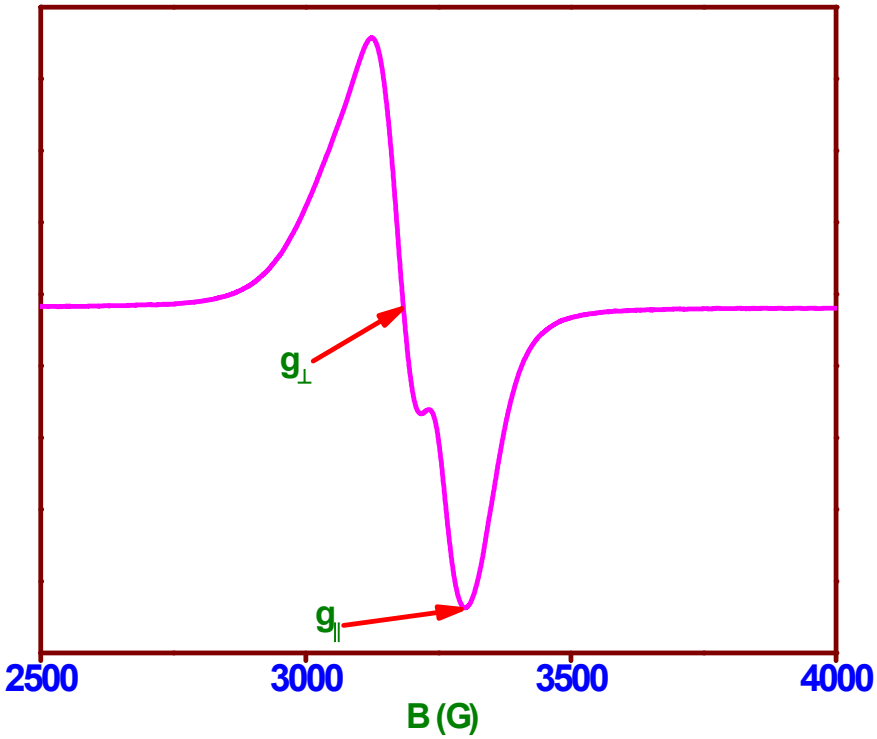

Fig. S8 Polycrystalline EPR spectra of [Cu(L^2)(phen)](ClO_4) (**2**) at room temperature.

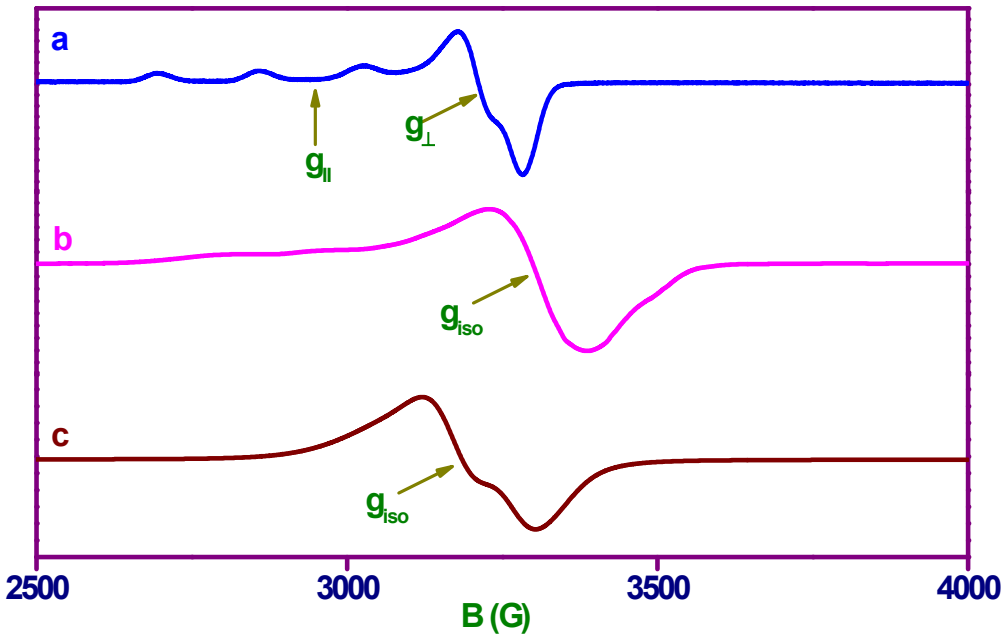

Fig. S9 EPR spectra for [Cu(L^1)(phen)](ClO_4) (**1**) at 77K: (a) DMF, (b) MeOH and (c) MeCN (concentration, 1×10^{-2} M).

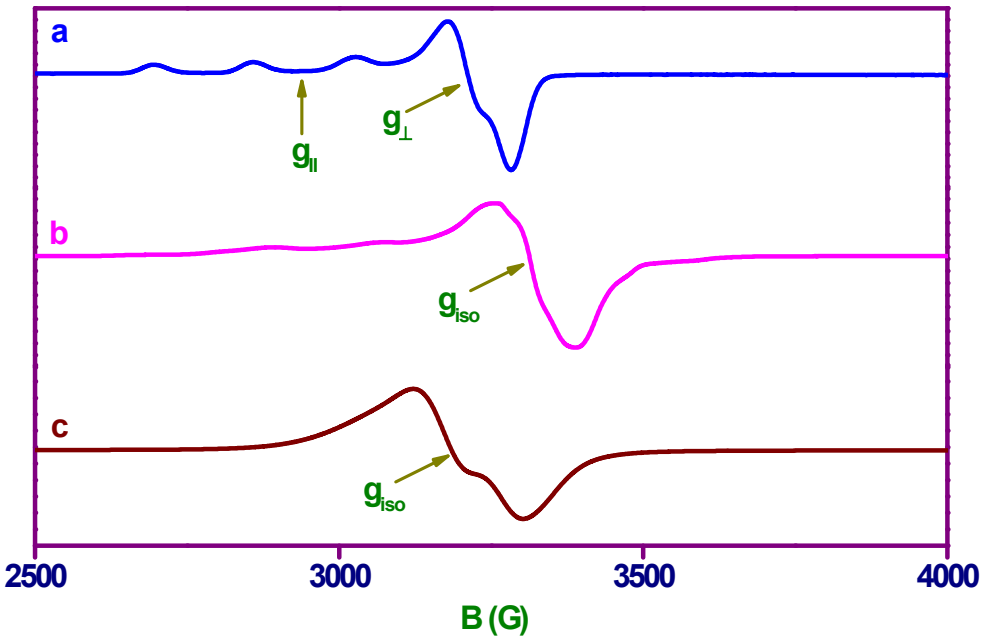

Fig. S10 EPR spectra for [Cu(L^2)(phen)](ClO_4) (**2**) at 77K: (a) DMF, (b) MeOH and (c) MeCN. (concentration, 1×10^{-2} M).

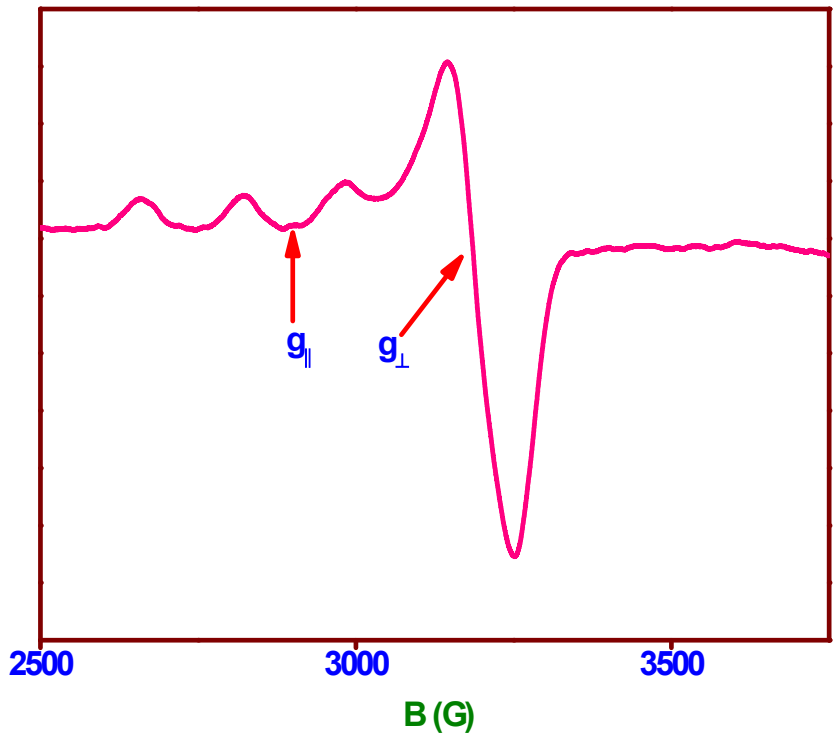

Fig. S11 EPR spectra for [Cu(L^1)(phen)](ClO_4) (**1**) at 77K in MeOH (concentration, 2.9×10^{-5} M).

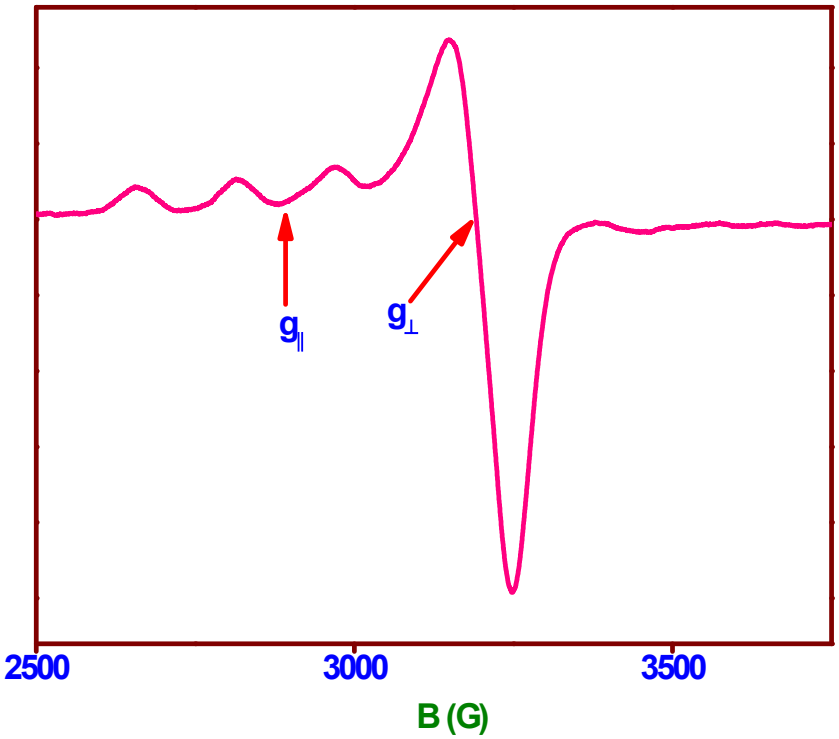

Fig. S12 EPR spectra for [Cu(L^1)(phen)](ClO_4) (**1**) at 77K in buffer solution (concentration, 2.9×10^{-5} M).

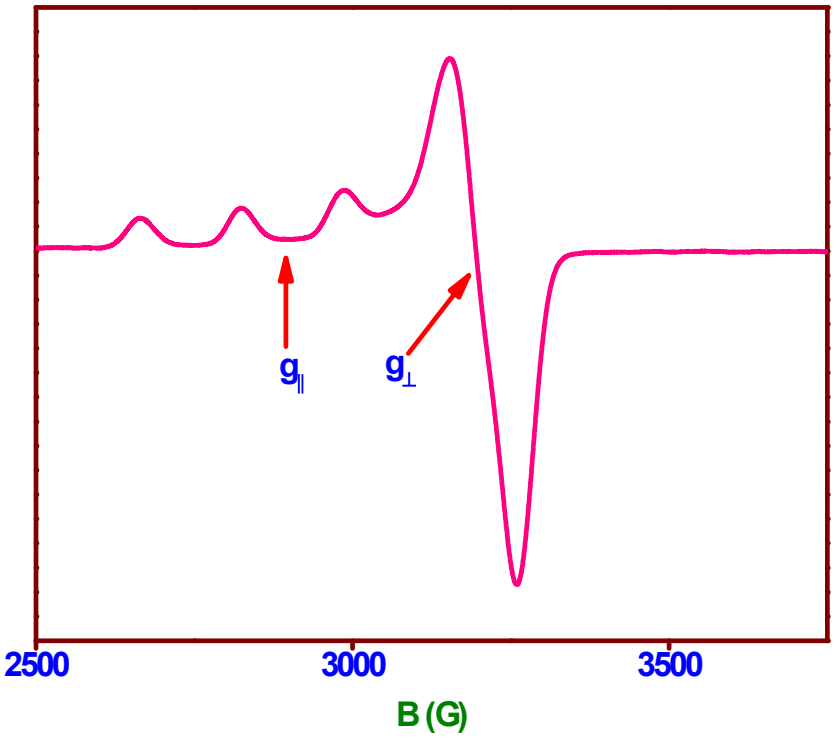

Fig. S13 EPR spectra for [Cu(L^2)(phen)](ClO_4) (**2**) at 77K in MeOH (concentration, 2.9×10^{-5} M).

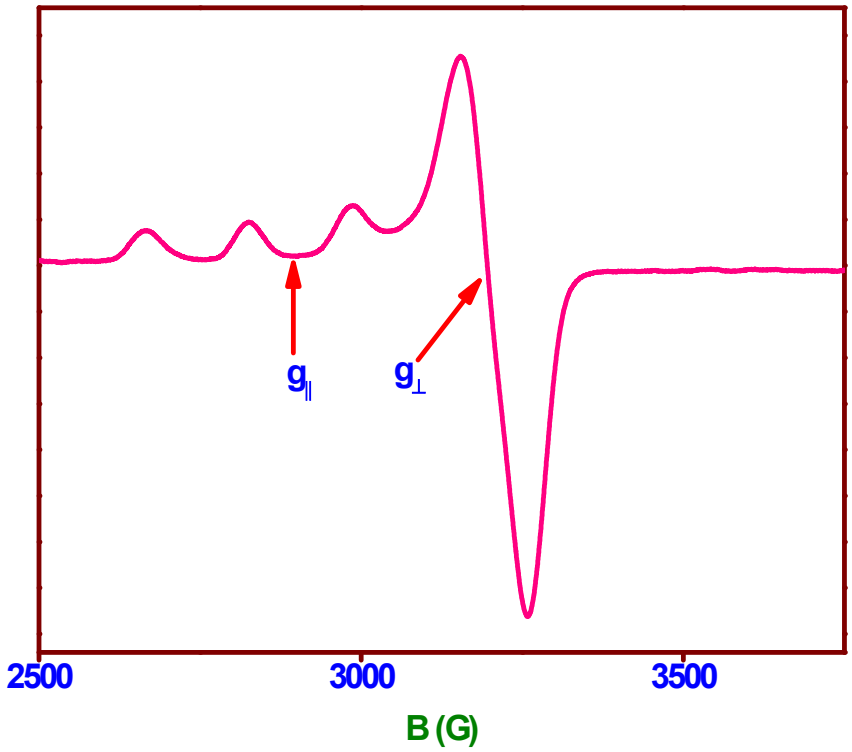

Fig. S14 EPR spectra for [Cu(L^2)(phen)](ClO_4) (**2**) at 77K in buffer solution (concentration, 2.9×10^{-5} M).

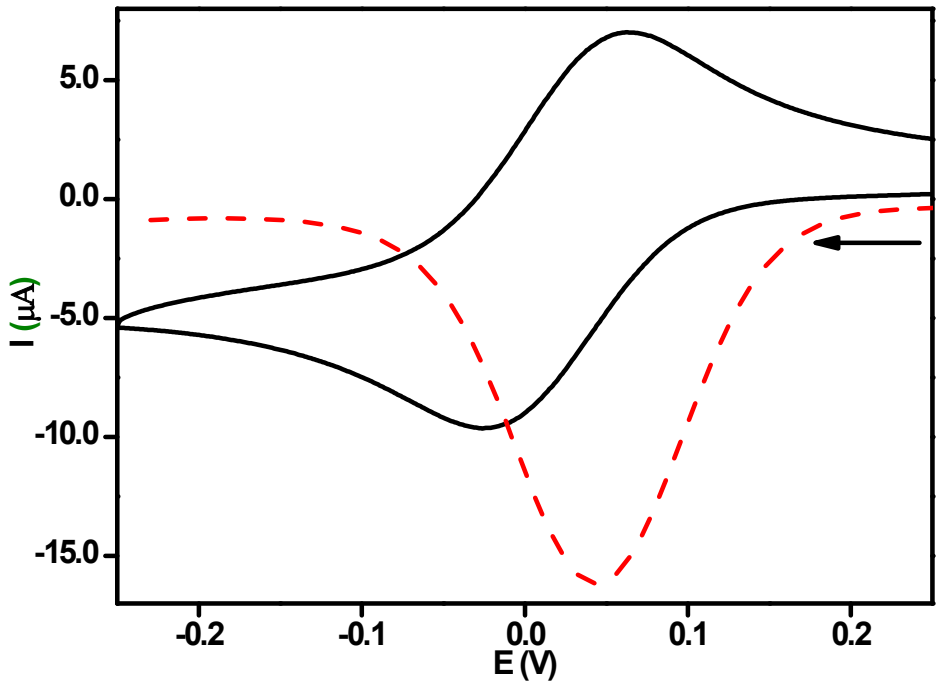

Fig. S15 Cyclic (CV) (——) and differential pulse (DPV) (-----) voltammograms of 0.001 M [Cu(L^1)(phen)](ClO_4) (**1**) in MeOH at 25 °C at 0.05 and 0.002 Vs^{-1} scan rates respectively.

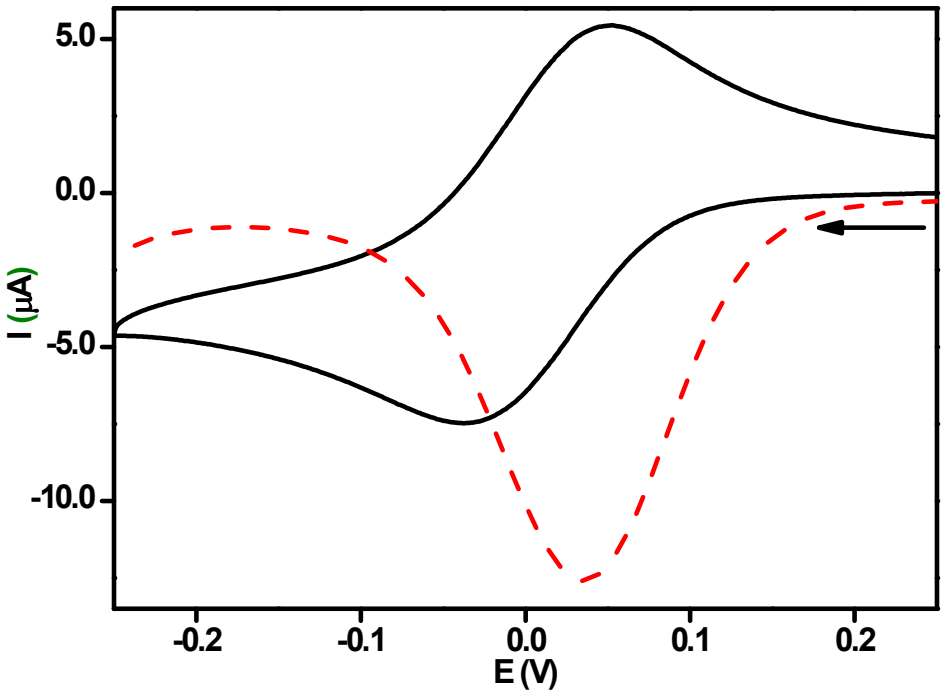

Fig. S16 Cyclic (CV) (——) and differential pulse (DPV) (-----) voltammograms of 0.001 M [Cu(L^2)(phen)](ClO_4) (**2**) in MeOH at 25 °C at 0.05 and 0.002 Vs^{-1} scan rates respectively.

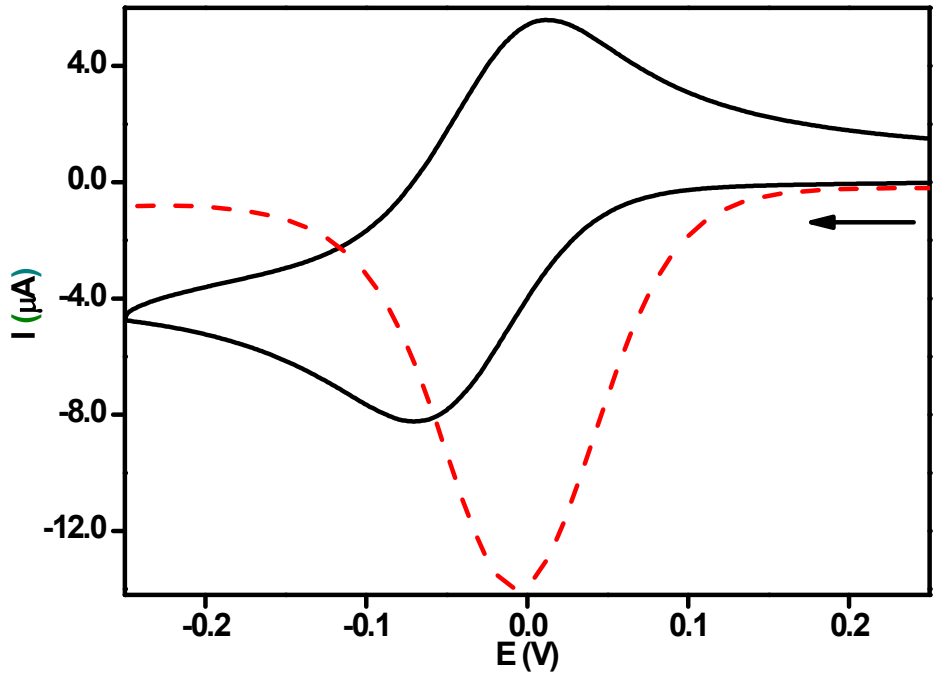

Fig. S17 Cyclic (CV) (——) and differential pulse (DPV) (-----) voltammograms of 0.001 M [Cu(L^1)(phen)](ClO_4) (**1**) in aq. MeOH at 25 °C at 0.05 and 0.002 Vs^{-1} scan rates respectively.

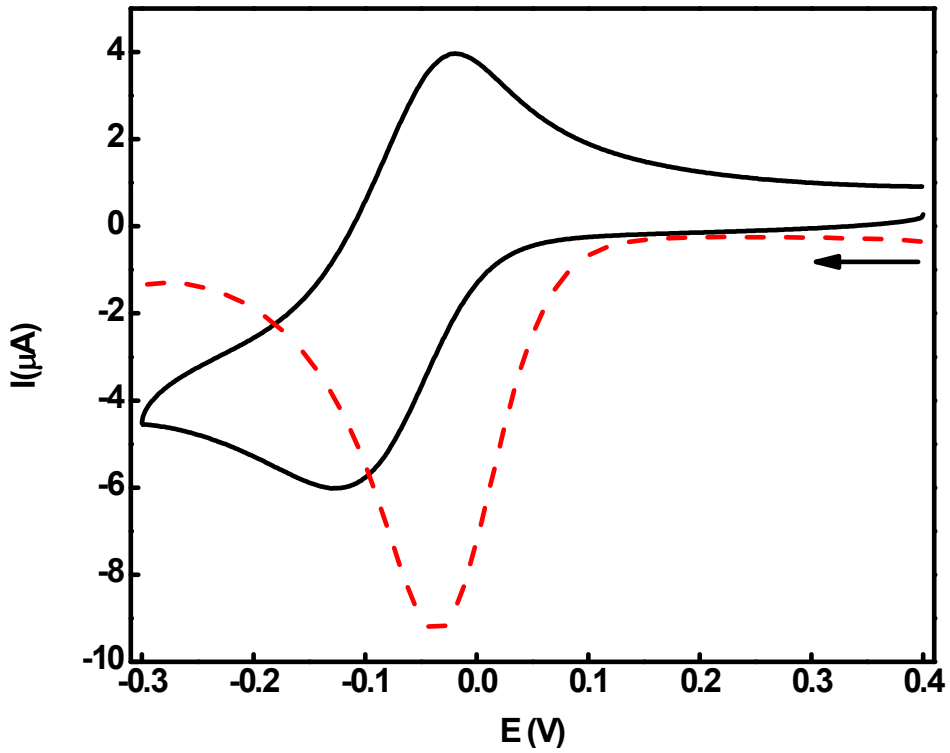

Fig. S18 Cyclic (CV) (——) and differential pulse (DPV) (-----) voltammograms of 0.001 M [Cu(L^2)(phen)](ClO_4) (**2**) in aq. MeOH at 25 °C at 0.05 and 0.002 Vs^{-1} scan rates respectively.

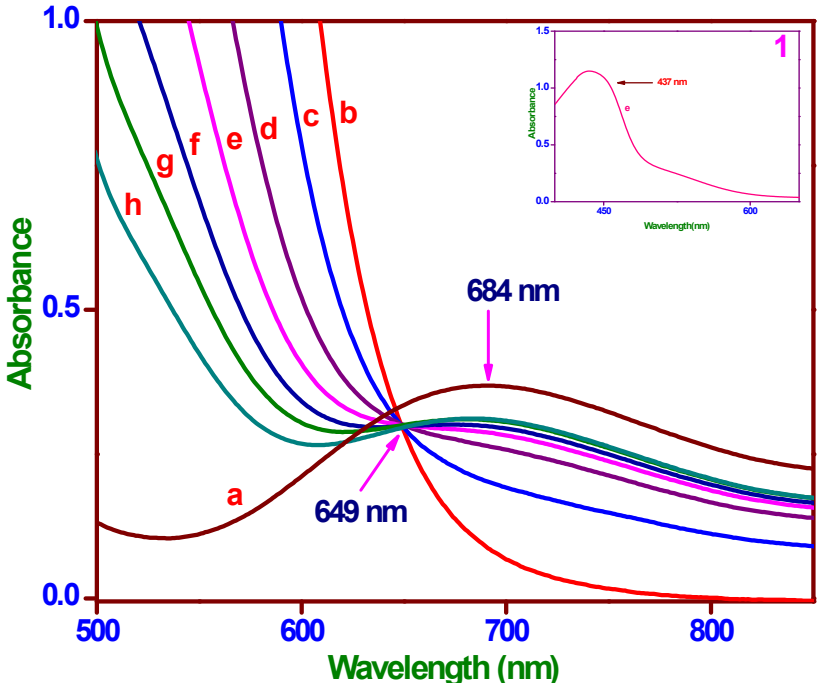

Fig. S19 Spectral trace of $[Cu^{II}(L^1)(phen)]+$ (**1**, 3×10^{-3} M) in MeOH:H_2O (4:1 v/v) in the visible region (spectrum a); Reduction of copper(II) to copper(I) (color change from green to brown) with addition of H_2A (3×10^{-3} M) up to 15 min (spectra b, c, d, and e); Regeneration of copper(II) species (color change from brown to green) from 20 to 30 min (spectra f, g, and h). Inset: generation of charge transfer band in brown solution due to formation of copper(I) species up to 15 min (spectrum e).

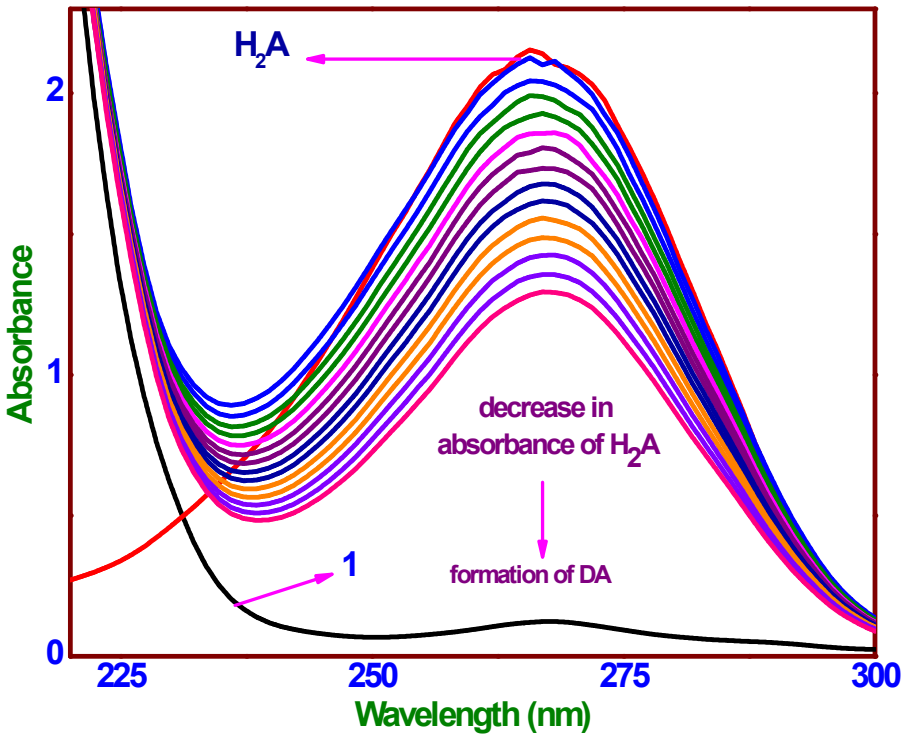

Fig. S20 UV-visible spectroscopy employed to monitor the oxidation of H_2A by $[Cu(L^1)(phen)](ClO_4)$ (**1**) in aq. MeOH.

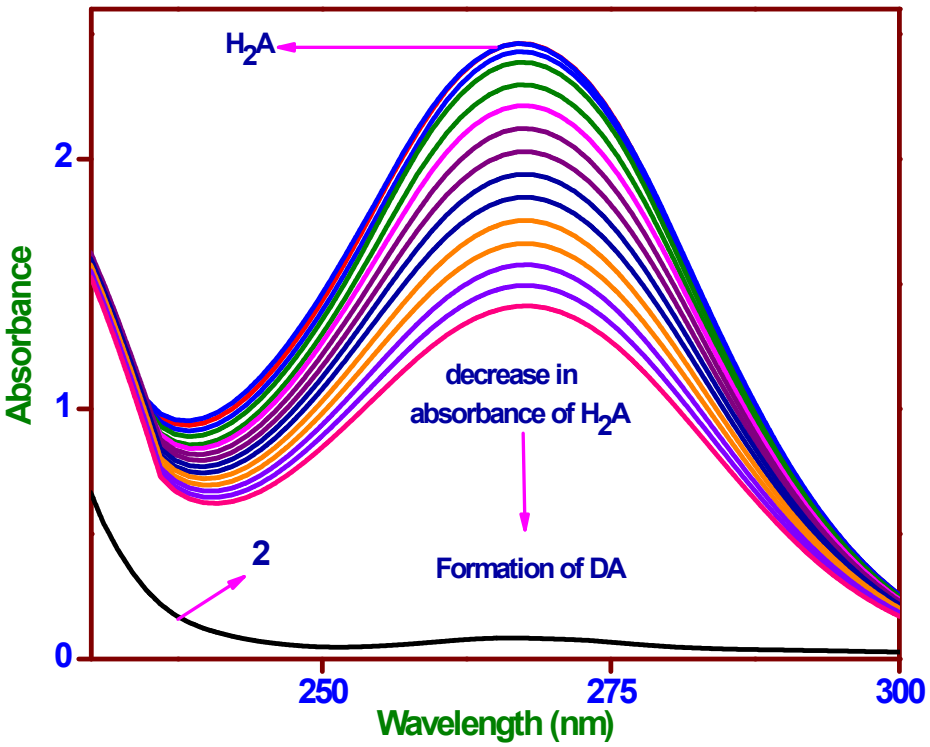

Fig. S21 UV-visible spectroscopy employed to monitor the oxidation of H_2A by $[Cu(L^2)(phen)](ClO_4)$ (**2**) in aq. MeOH.

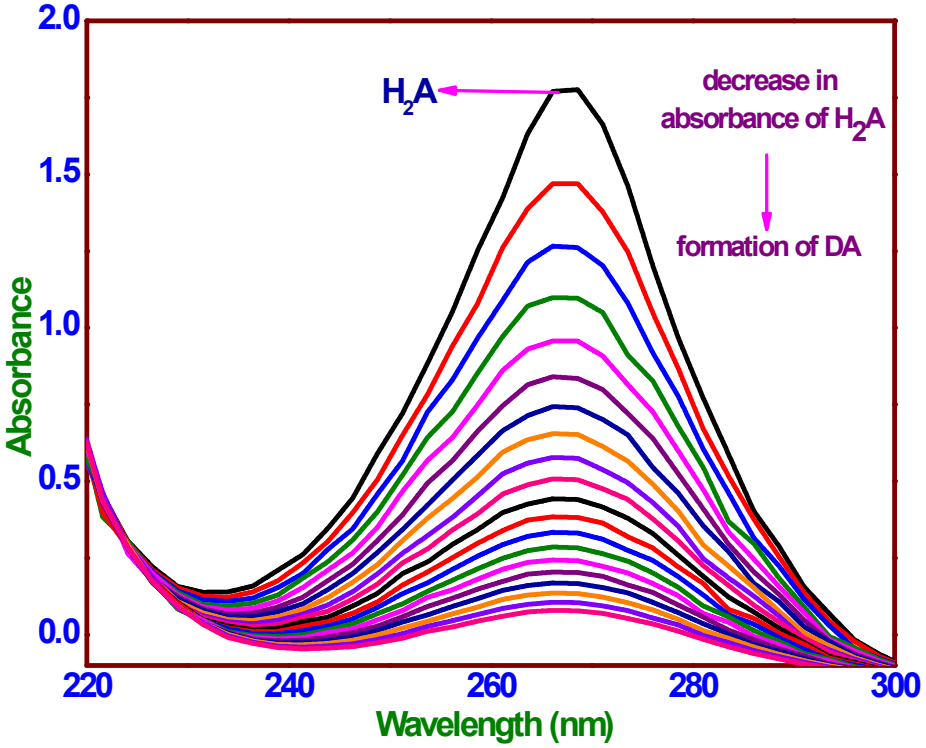

Fig. S22 UV-visible spectroscopy employed to monitor the oxidation of H_2A by $[Cu(L^1)(phen)](ClO_4)$ (**1**) in buffer solution (pH 7.6).

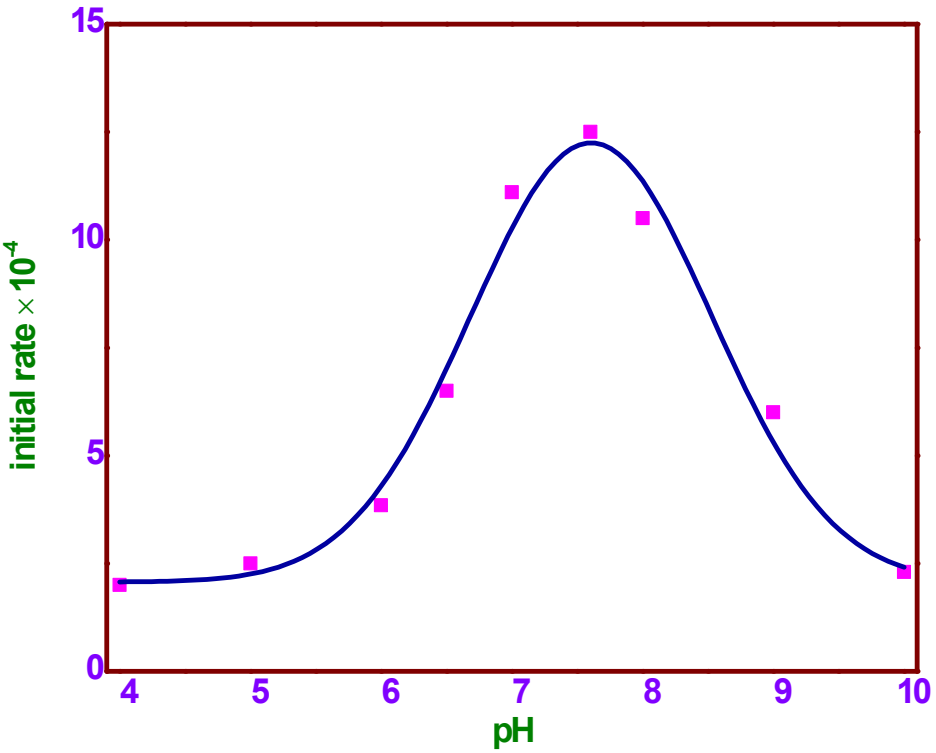

Fig. S23 Graph of initial rate as a function of pH for the oxidation of H_2A catalyzed by $[Cu(L^1)(phen)](ClO_4)$ (**1**) in aq. MeOH at 25 °C under the following conditions: [complex] = 1.66×10^{-6} M; [H_2A] = 8.3×10^{-5} M; [buffers] = 0.1 M without ionic strength.

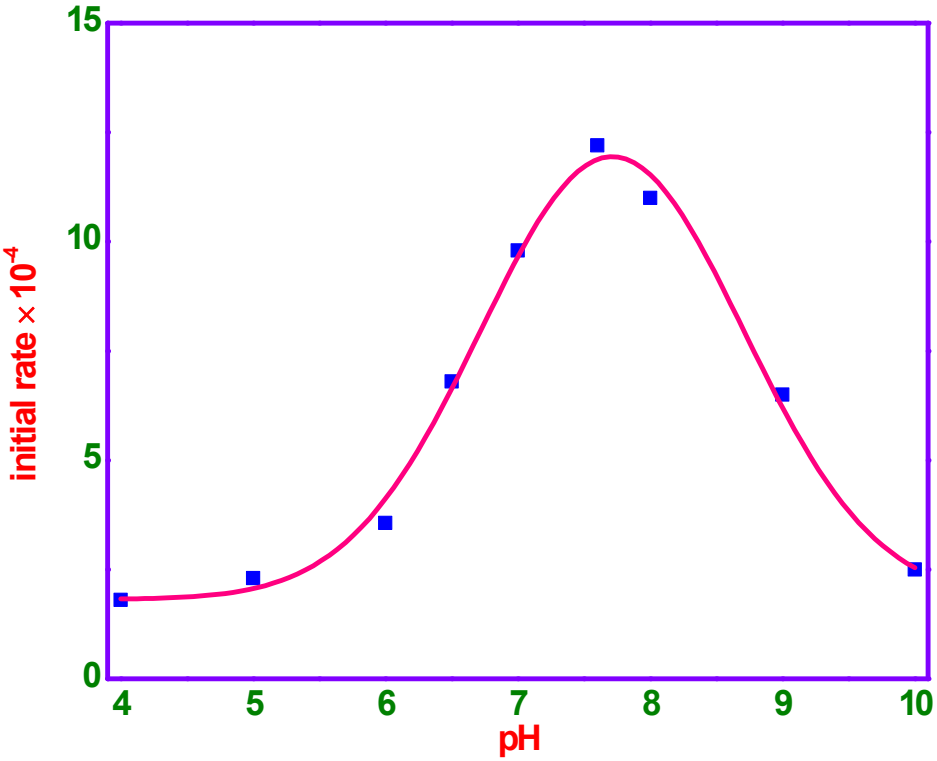

Fig. S24 Graph of initial rate as a function of pH for the oxidation of H_2A catalyzed by $[Cu(L^2)(phen)](ClO_4)$ (**2**) in aq. MeOH at 25 °C under the following conditions: [complex] = 1.66×10^{-6} M; [H_2A] = 8.3×10^{-5} M; [buffers] = 0.1 M without ionic strength

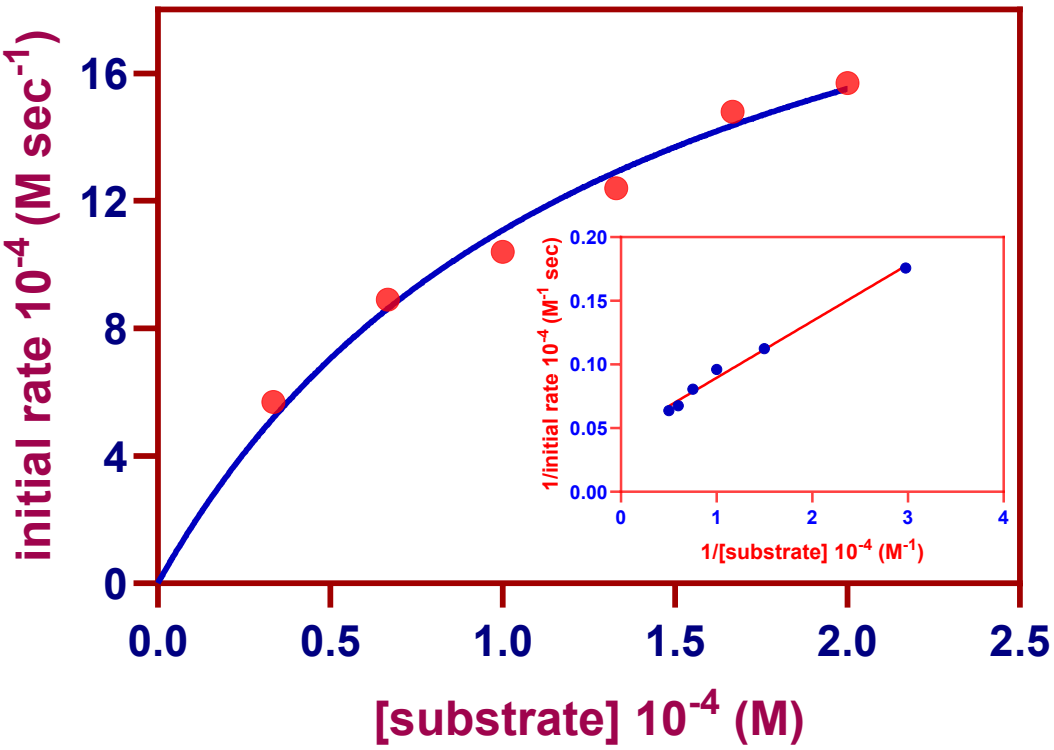

Fig. S25 Reaction rates for the oxidation reaction catalyzed by $[Cu(L^1)(phen)](ClO_4)$ (**1**) depend on the concentration of H_2A in aq. MeOH. Inset: Lineweaver-Burk plot.

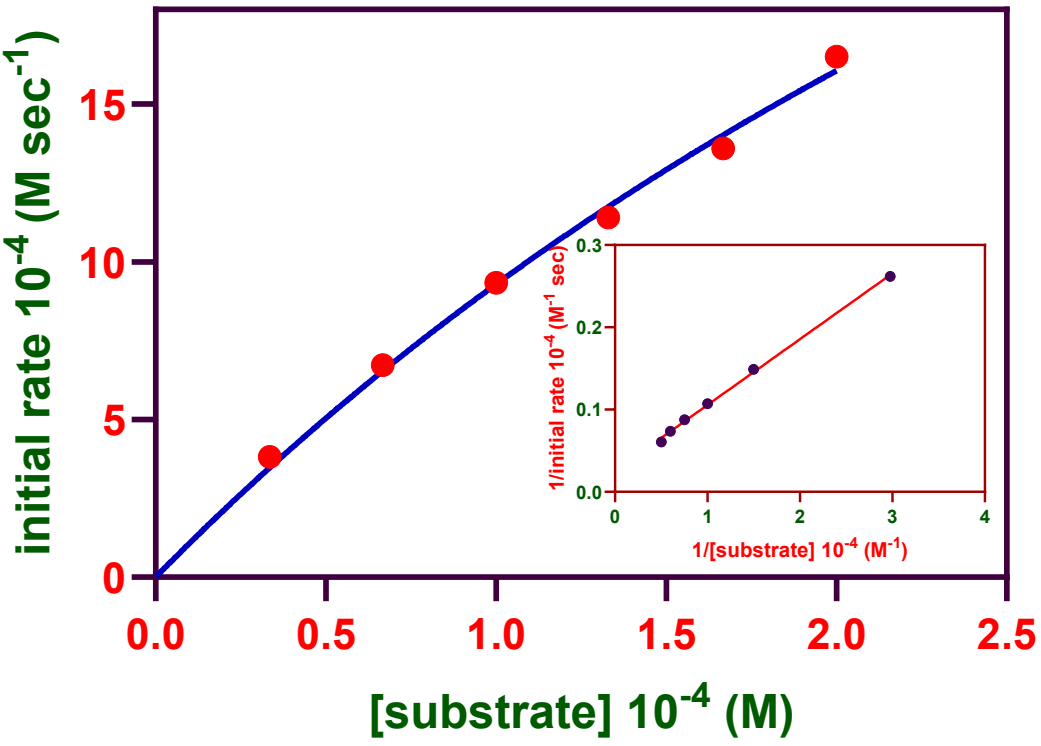

Fig. S26 Reaction rates for the oxidation reaction catalyzed by $[Cu(L^2)(phen)](ClO_4)$ (**2**) depend on the concentration of H_2A in aq. MeOH. Inset: Lineweaver-Burk plot.

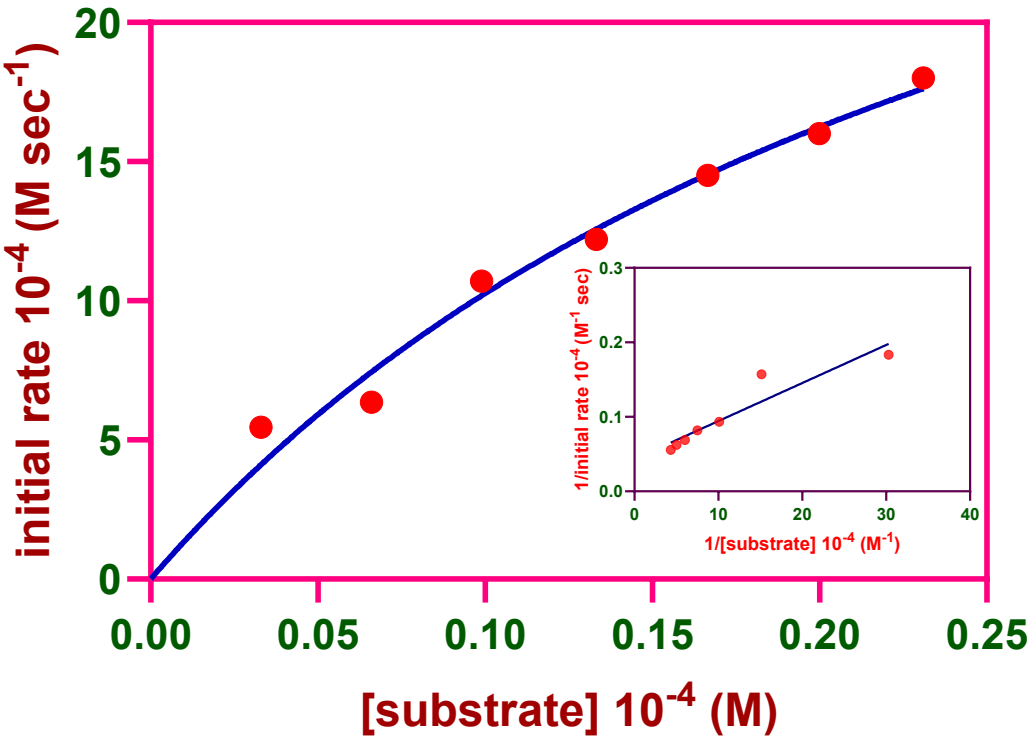

Fig. S27 Reaction rates for the oxidation reaction catalyzed by [Cu(L^1)(phen)](ClO_4) (**1**) depend on the concentration of H_2A in buffer solution (pH 7.6).
Inset: Lineweaver-Burk plot.

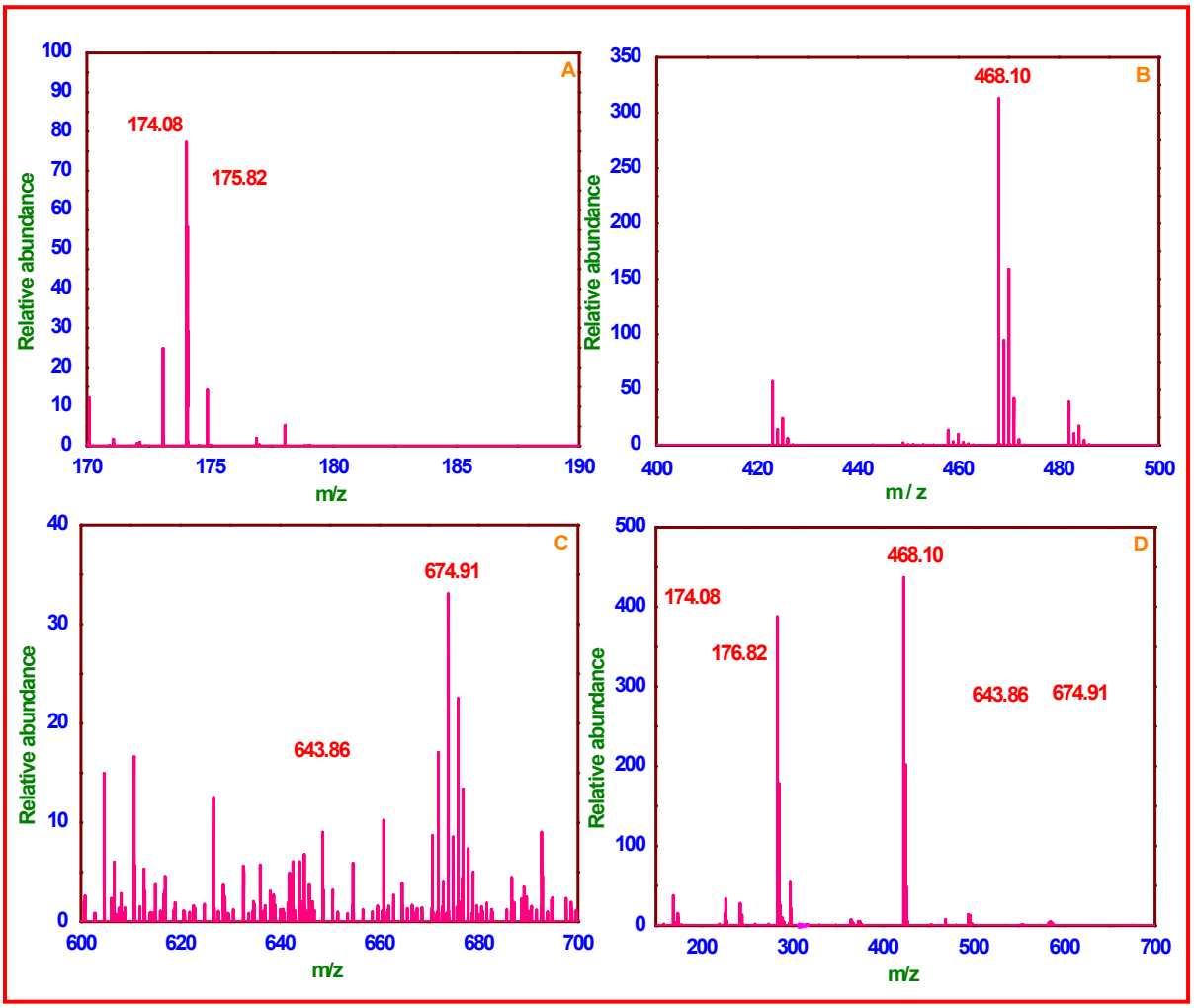

Fig. S28 HRMS spectra of a mixture containing $[Cu(L^2)(phen)](ClO_4)$ (**2**)and H_2A (molar ratio, 1:50) after 10 minutes. (A) m/z 170-190, (B) m/z 400-500, (C) m/z 600-700 and (D) full mass spectrum.

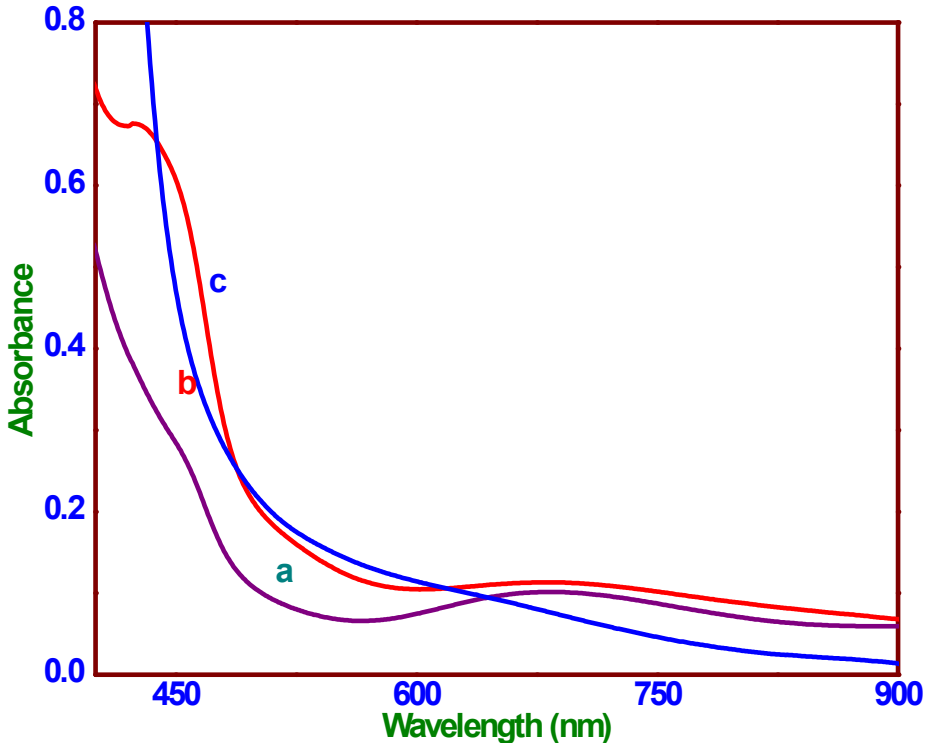

Fig. S29 Visible spectra of [Cu(L^1)(phen)](ClO_4) (**1**) in MeOH:H_2O (4:1 v/v) (a), with benzylamine present (b), and following benzylamine and H_2O_2 treatment (c).

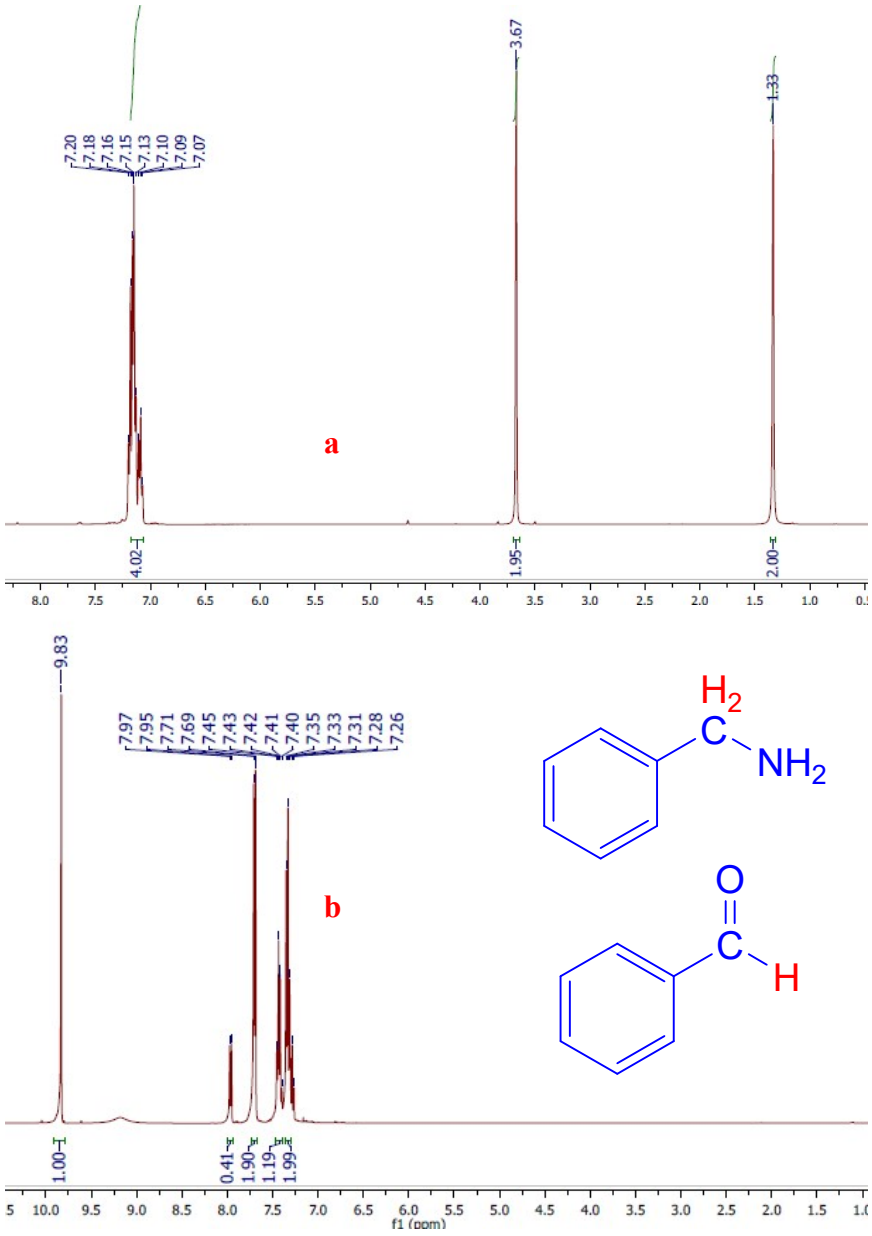

Fig. S30 ^{1}H NMR signals of (a) -CH_2- (benzylamine), δ 3.67 ppm and (b) -CHO (benzaldehyde), δ 9.83 ppm {catalyst, [Cu(L^2)(phen)](ClO_4)(**2**)}.

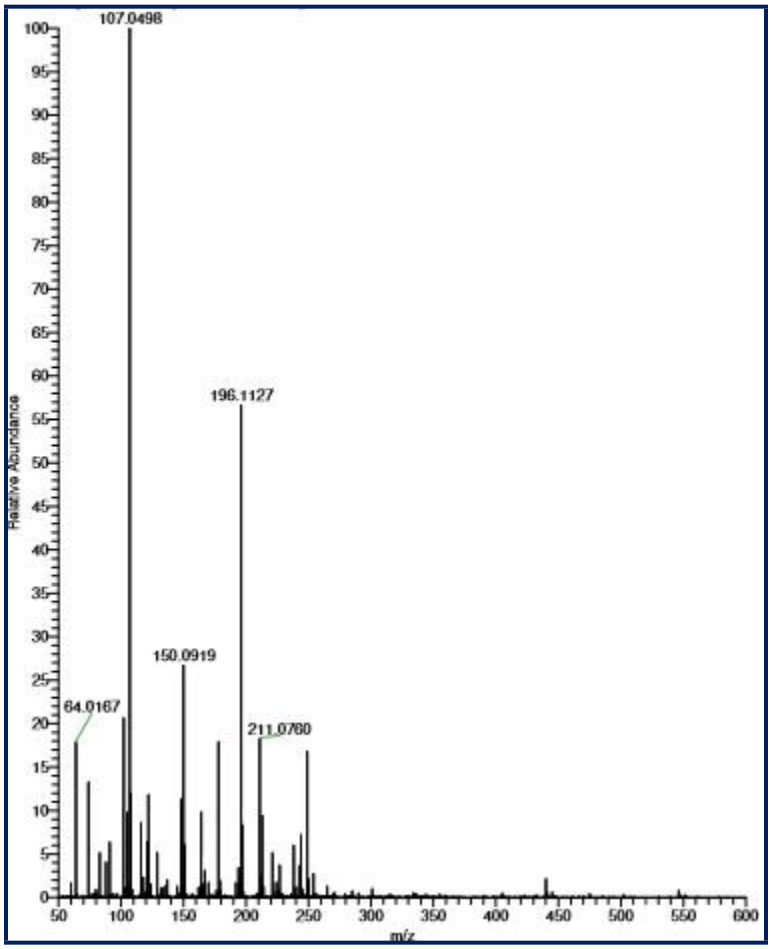

Fig. S31 HRMS of benzaldehyde, which is extracted from the reaction mixture with the aid of $[Cu(L^2)(phen)](ClO_4)$ (**2**), a catalyst.

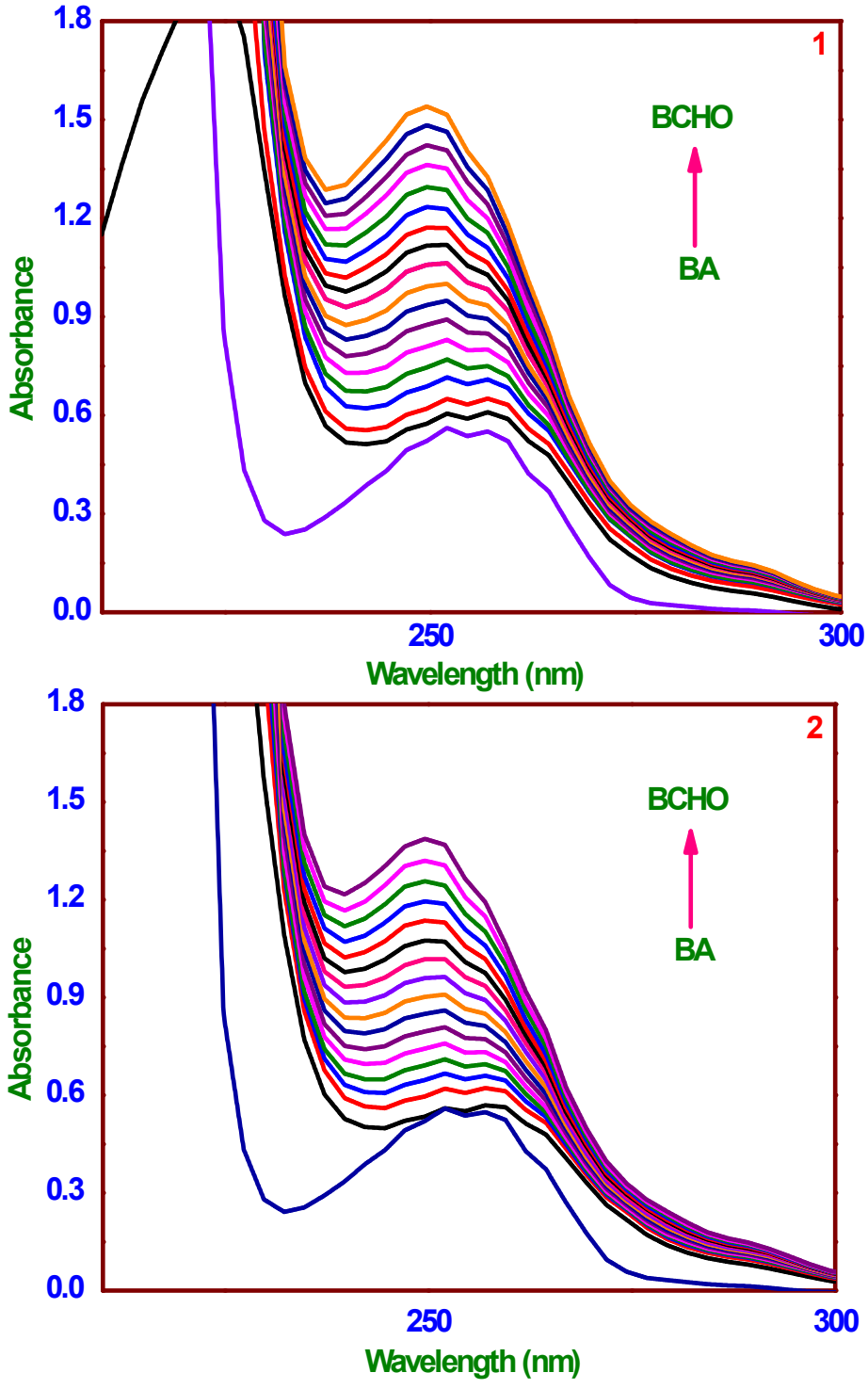

Fig. S32 UV-visible spectroscopy employed to monitor the oxidation of Ph-CH_2-NH_2 by $[Cu(L^1/L^2)(phen)](ClO_4)$ (**1**,**2**) in aq, MeOH.

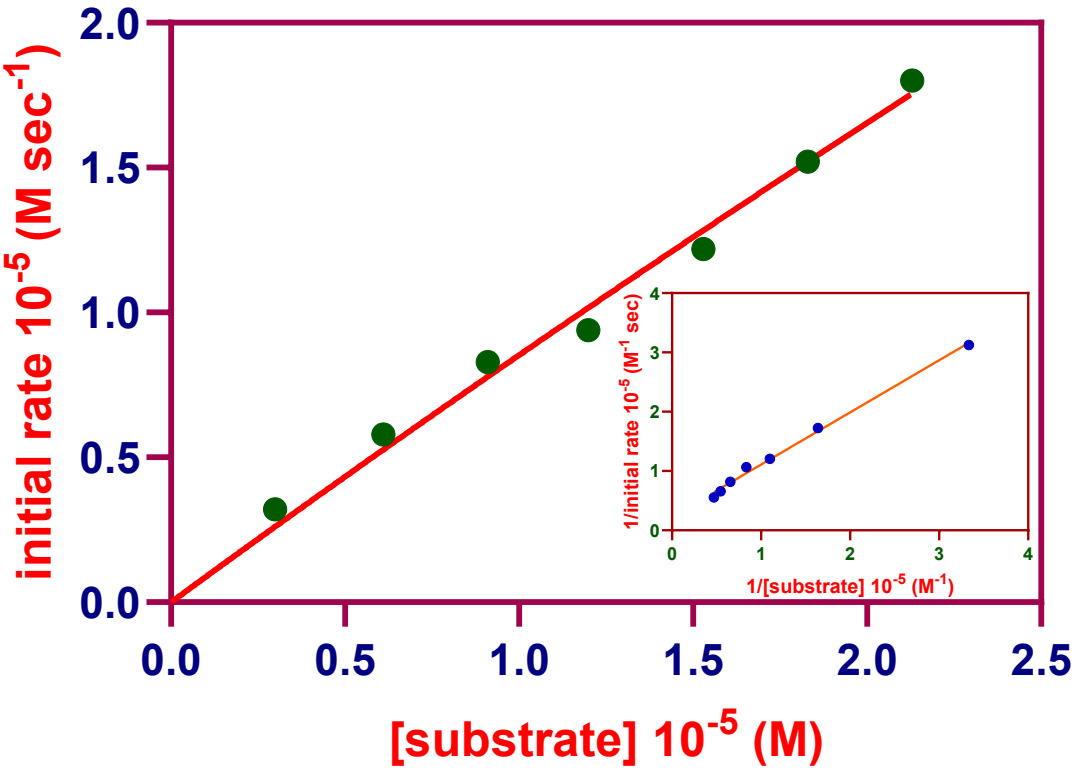

Fig. S33 Reaction rates for the oxidation reaction catalyzed by [Cu(L^1)(phen)](ClO_4) (**1**) depend on the concentration of Ph-CH_2-NH_2. Inset: Lineweaver-Burk plot.

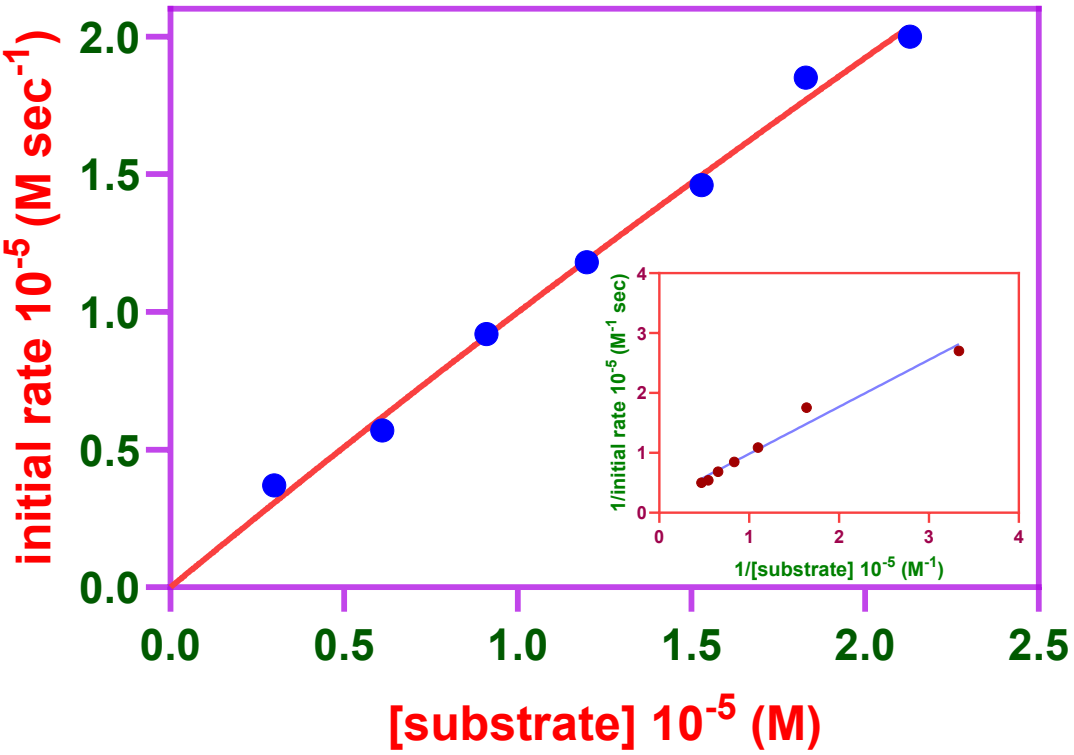

Fig. S34 Reaction rates for the oxidation reaction catalyzed by $[Cu(L^2)(phen)](ClO_4)$ (**2**) depend on the concentration of Ph-CH_2-NH_2. Inset: Lineweaver-Burk plot.

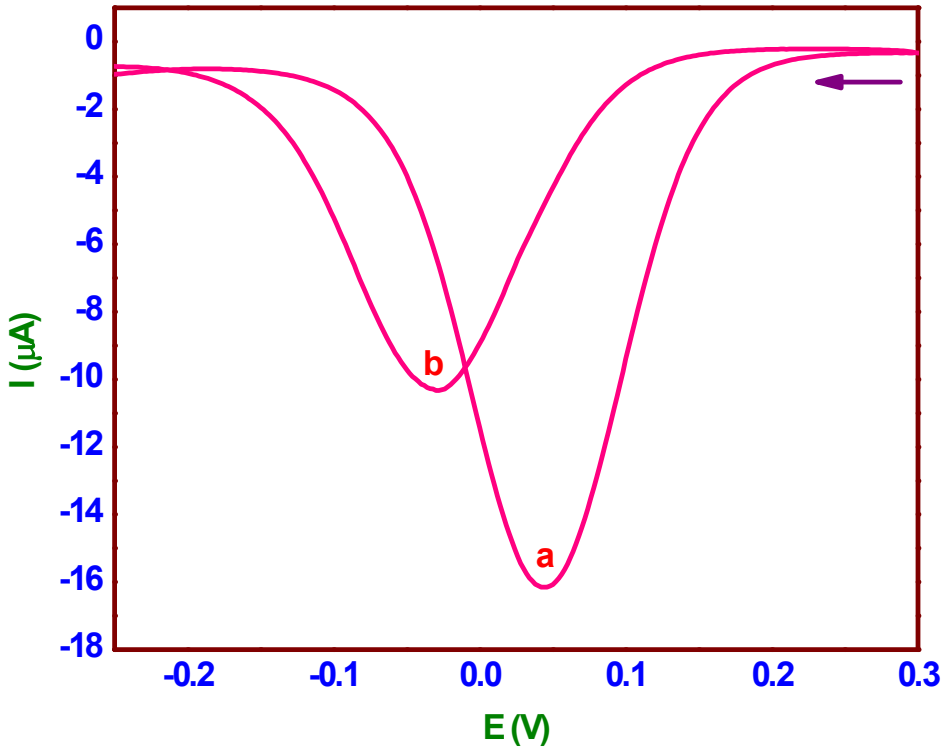

Fig. S35 Differential pulse voltammogram of [Cu(L^1)(phen)](ClO_4)(**1**) (a) upon addition of benzylamine (molar ratio, 1:5) (b).

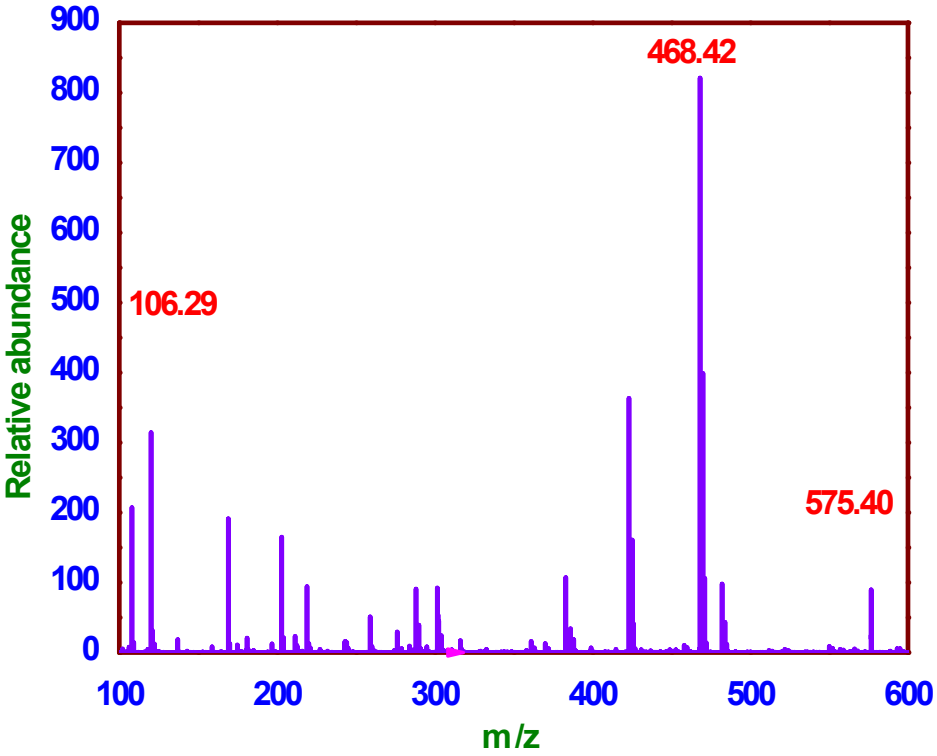

Fig. S36 HRMS spectra of a mixture containing $[Cu(L^2)(phen)](ClO_4)$ and $PhCH_2NH_2$ (molar ratio, 1:50) after 10 minutes.

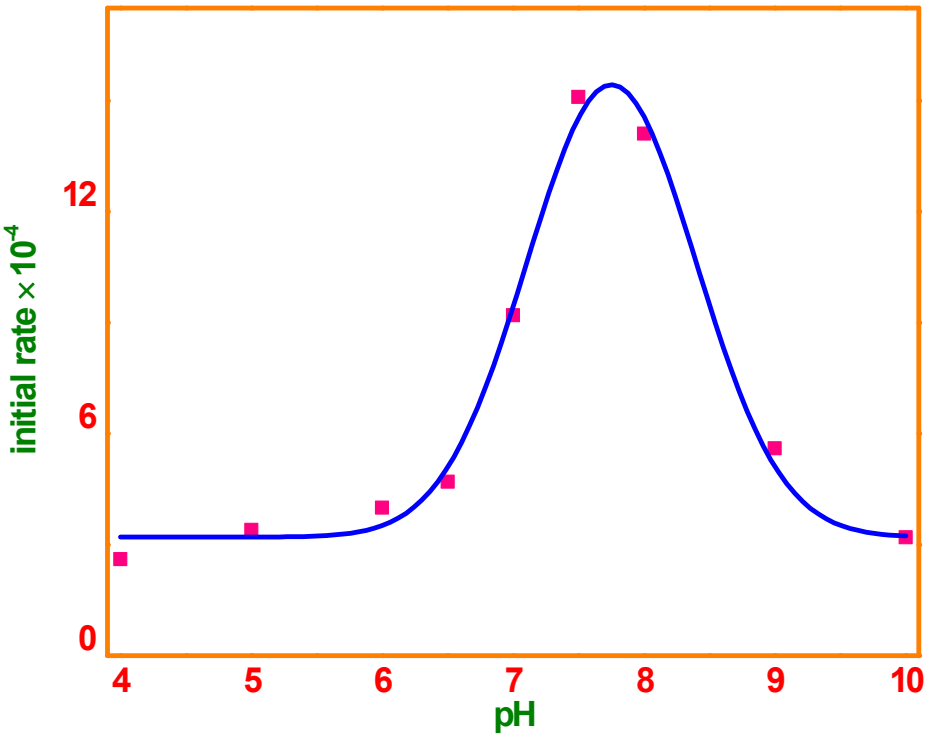

Fig. S37 Graph of intial rate as a function of pH for the oxidation of 3,5-DTBC catalyzed by $[Cu(L^1)(phen)](ClO_4)$ (**1**) in buffer solution (4-10) at 25 °C under the following conditions: $[Cu(L^1)(phen)](ClO_4) = 2.9 \times 10^{-5}$ M; [3,5-DTBC] = 1.45×10^{-3} M; [buffer solution] = 0.1 M without ionic strength.

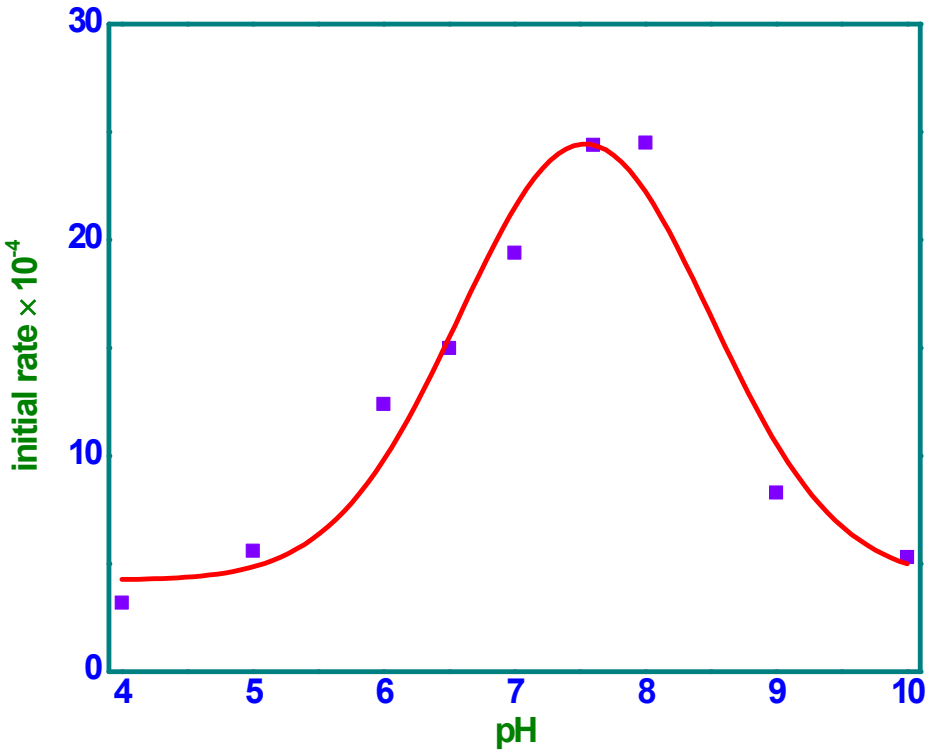

Fig. S38 Graph of intial rate as a function of pH for the oxidation of 3,5-DTBC catalyzed by $[Cu(L^2)(phen)](ClO_4)$ (**2**) in buffer solution (4-10) at 25 °C under the following conditions: $[Cu(L^2)(phen)](ClO_4) = 2.9 \times 10^{-5}$ M; [3,5-DTBC] = 1.45×10^{-3} M; [buffer solution] = 0.1 M without ionic strength.

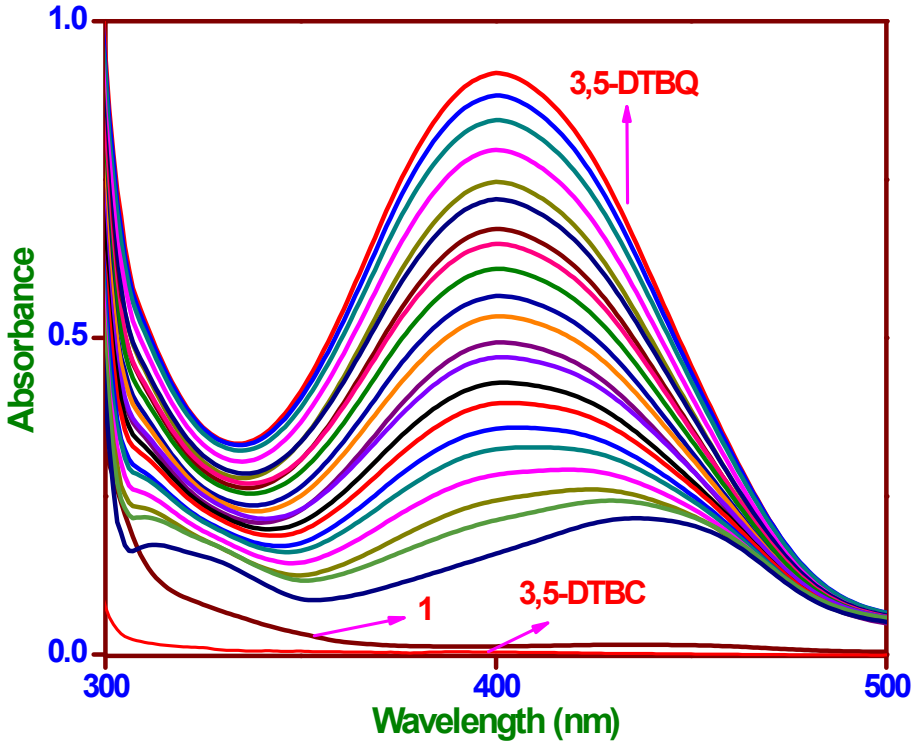

Fig. S39 Oxidation of 3,5-DTBC by [Cu(L^1)(phen)](ClO_4) (**1**) in MeOH monitored by UV-Vis spectroscopy.

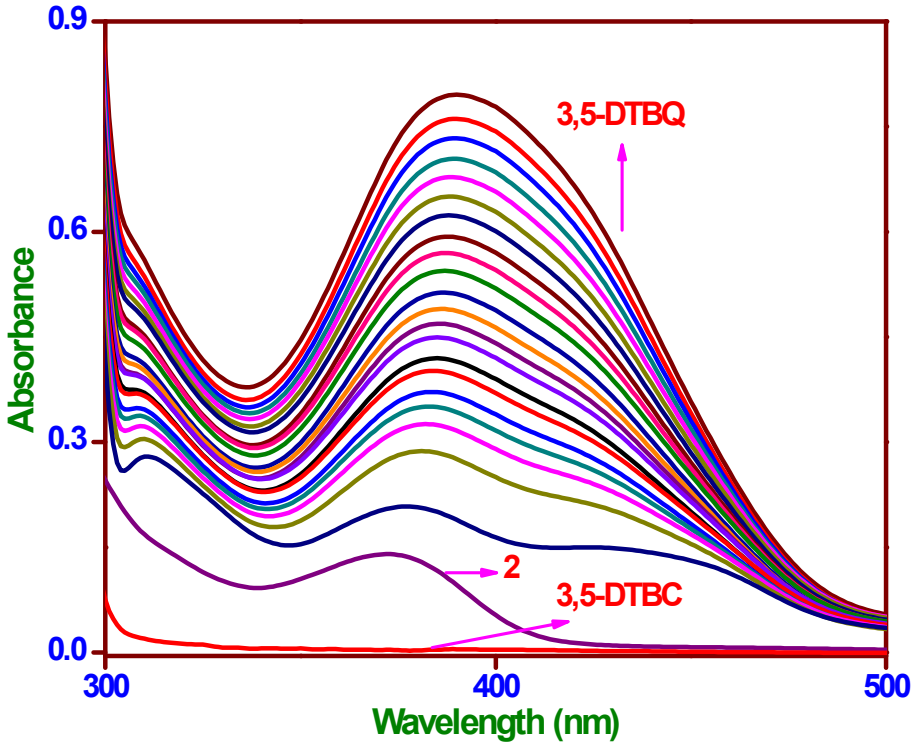

Fig. S40 Oxidation of 3,5-DTBC by [Cu(L^2)(phen)](ClO_4) (**2**) in MeOH monitored by UV-Vis spectroscopy.

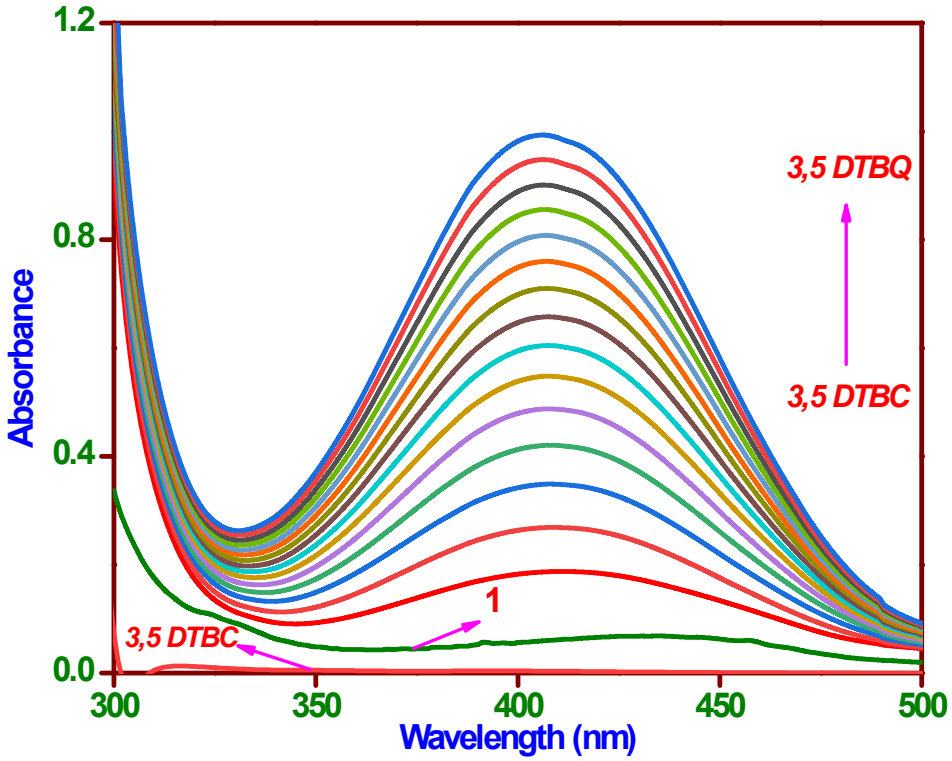

Fig. S41 The increase in the formation of 3,5-DTBQ monitored spectrophotometrically by the oxidation of 3,5-DTBC using the catalyst, $[Cu(L^1)(phen)](ClO_4)$ (**1**) in buffer solution (pH 7.6).

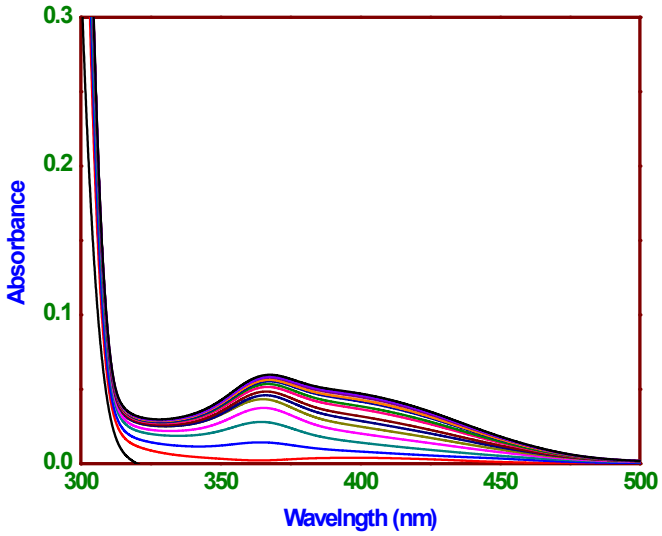

Fig. S42 The autoxidation of 3,5-DTBC monitored spectrophotometrically in MeOH.

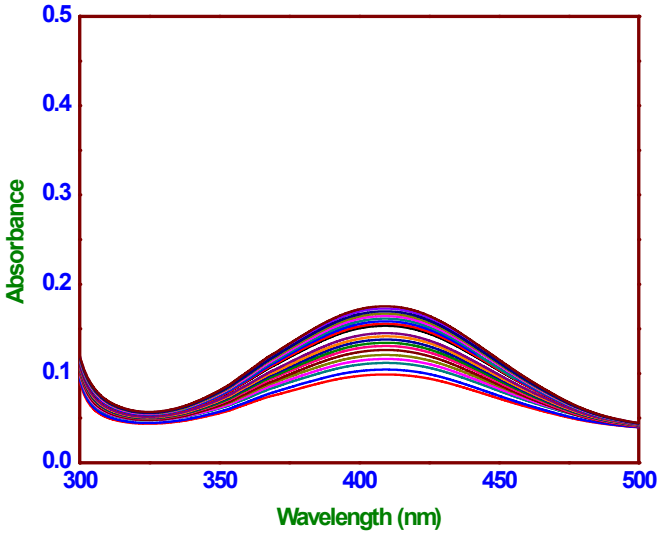

Fig. S43 The autoxidation of 3,5-DTBC monitored spectrophotometrically in buffer solution.

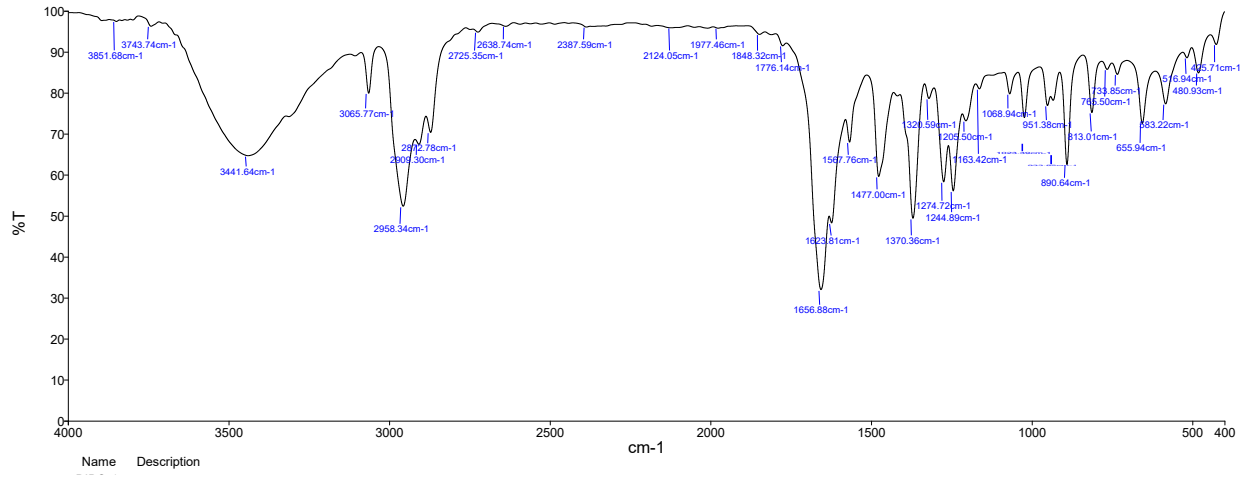

Fig. S44 FTIR spectrum of 3,5-DTBQ after separated from the reaction mixture using a catalyst, $[Cu(L^2)(phen)](ClO_4)$ (**2**).

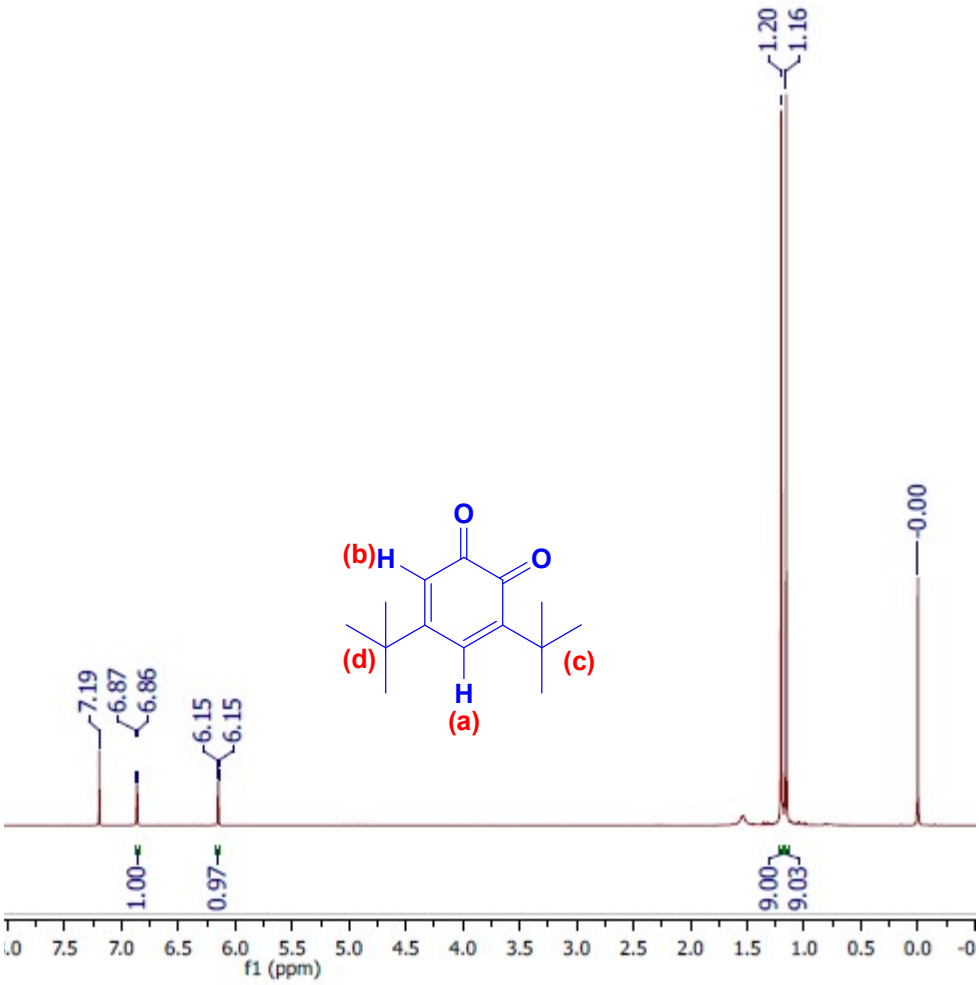

Fig. S45 ^{1}H NMR signals of 3,5-DTBQ after separated from the reaction mixture using a catalyst, [Cu(L^2)(phen)](ClO_4) (**2**).

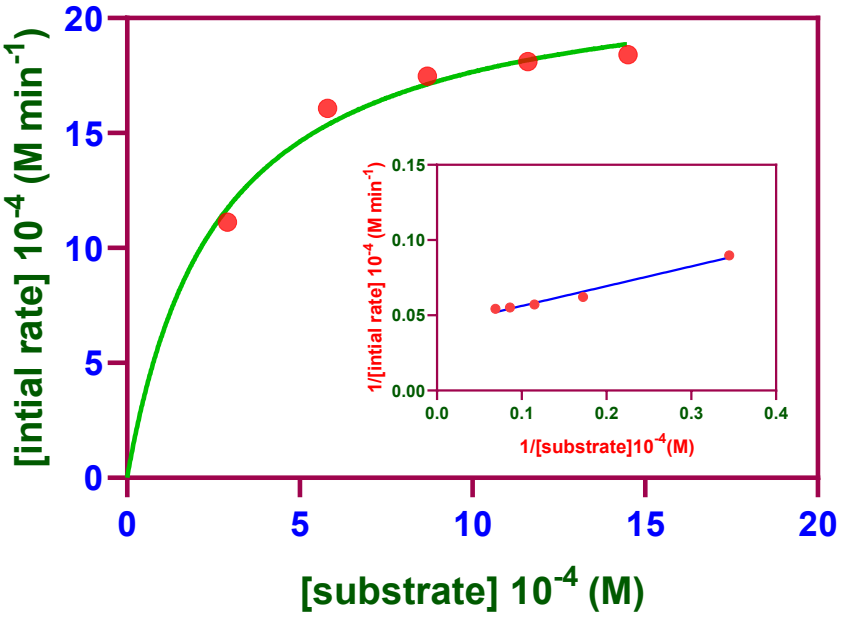

Fig. S46 Dependence of reaction rates on the 3,5-DTBC concentration for the oxidation reaction catalyzed by $[Cu(L^1)(phen)](ClO_4)$ (**1**). Inset: Lineweaver-Burk plot.

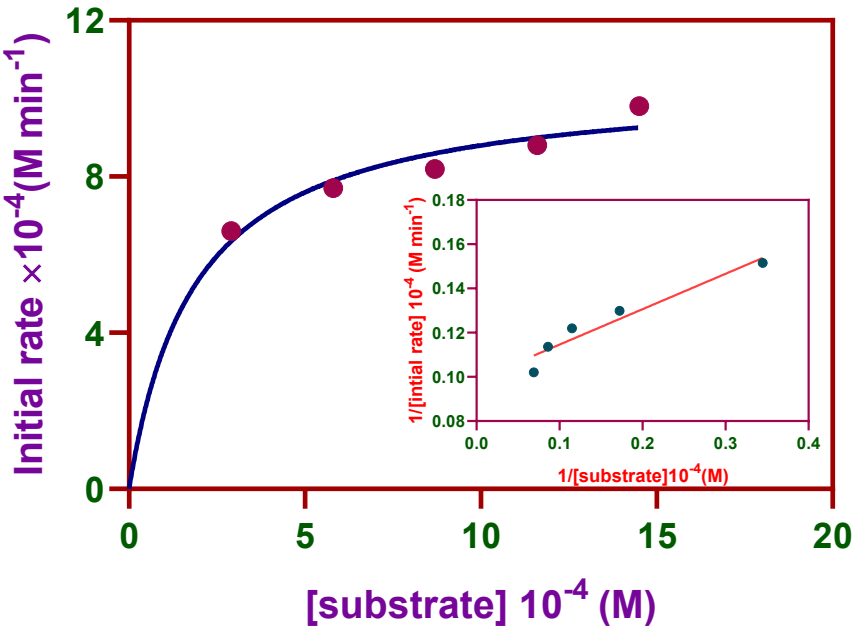

Fig. S47 Dependence of reaction rates on the 3,5-DTBC concentration for the oxidation reaction catalyzed by $[Cu(L^2)(phen)](ClO_4)$ (**2**). Inset: Lineweaver-Burk plot.

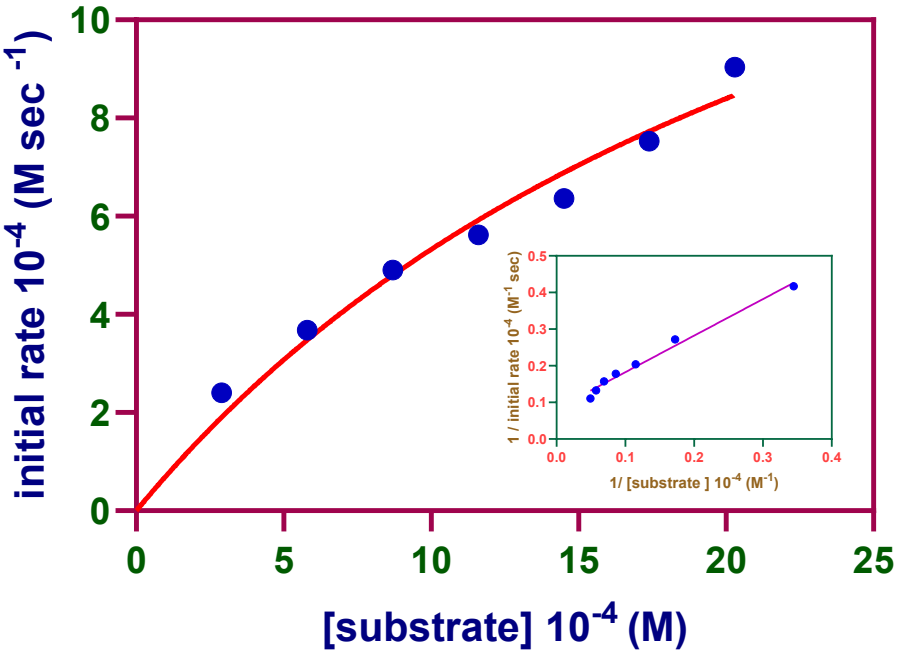

Fig. S48 The initial rate plots as a function of the substrate concentration for the oxidation of 3,5-DTBC, catalyzed by $[Cu(L^1)(phen)](ClO_4)$ (**1**) in buffer solution (pH 7.6). Inset: Lineweaver-Burk plot.

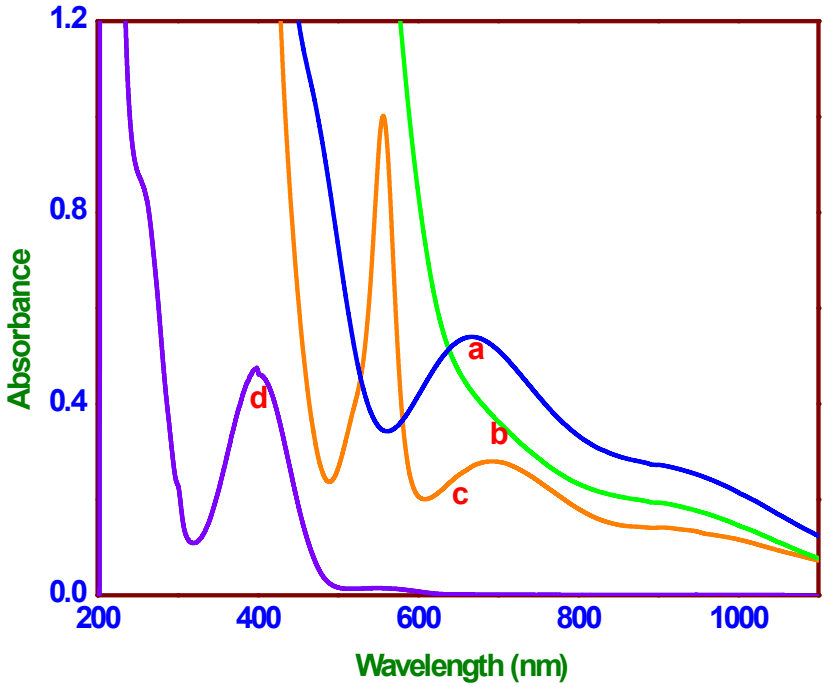

Fig. S49 Electronic spectral changes of [Cu(L^1)(phen)](ClO_4) (**1**) (3.2×10^{-3} M) upon addition of 3,5-DTBC (molar ratio, 1:100) in MeOH. Electronic spectrum of complex (a), disappearance of d-d band immediately after the addition of 3,5-DTBC (b), formation of superoxide intermediate (c) and generation of 3,5-DTBQ (d).

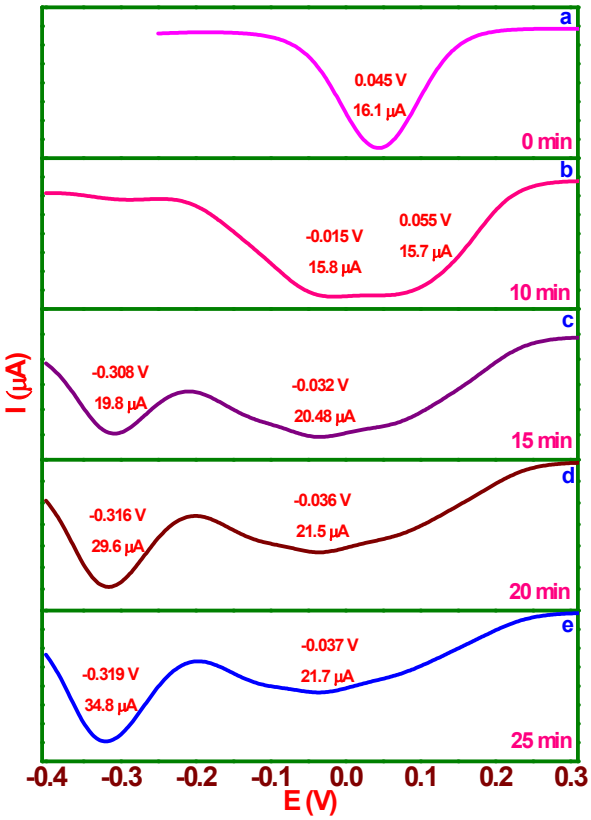

Fig. S50 Changes in differential pulse voltammograms of [Cu(L^1)(phen)](ClO_4) (**1**) after \ adding 3,5-DTBC (stoichiometry equivalent, 1:5; time interval, 5 min).

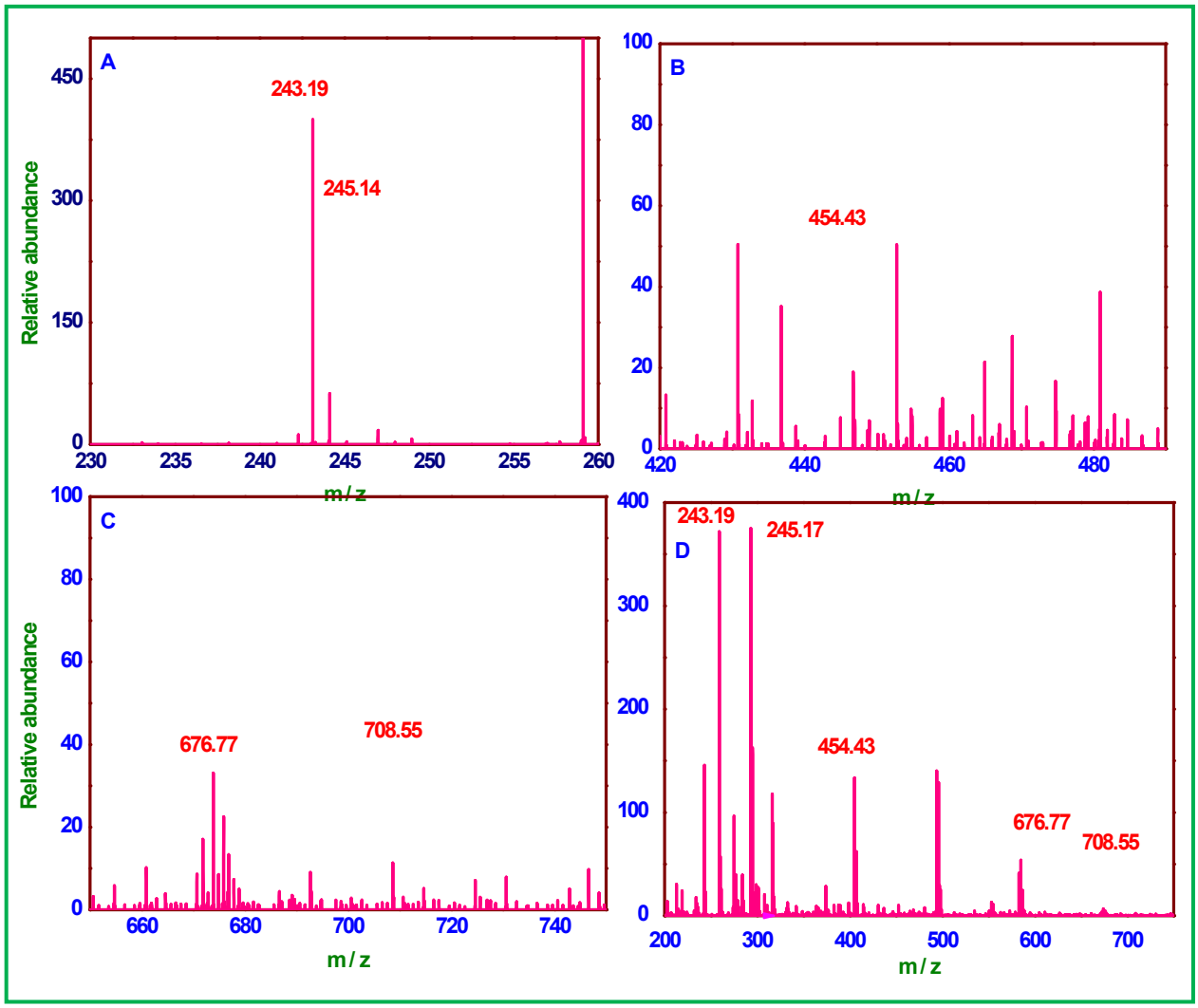

Fig. S51 HRMS spectra of a mixture containing $[Cu(L^1)(phen)](ClO_4)$ (**1**) and H_2A (molar ratio, 1:50) after 10 minutes in MeOH. (A) m/z 230-260, (B) m/z 420-500, (C) m/z 650-750 and (D) full mass spectrum.

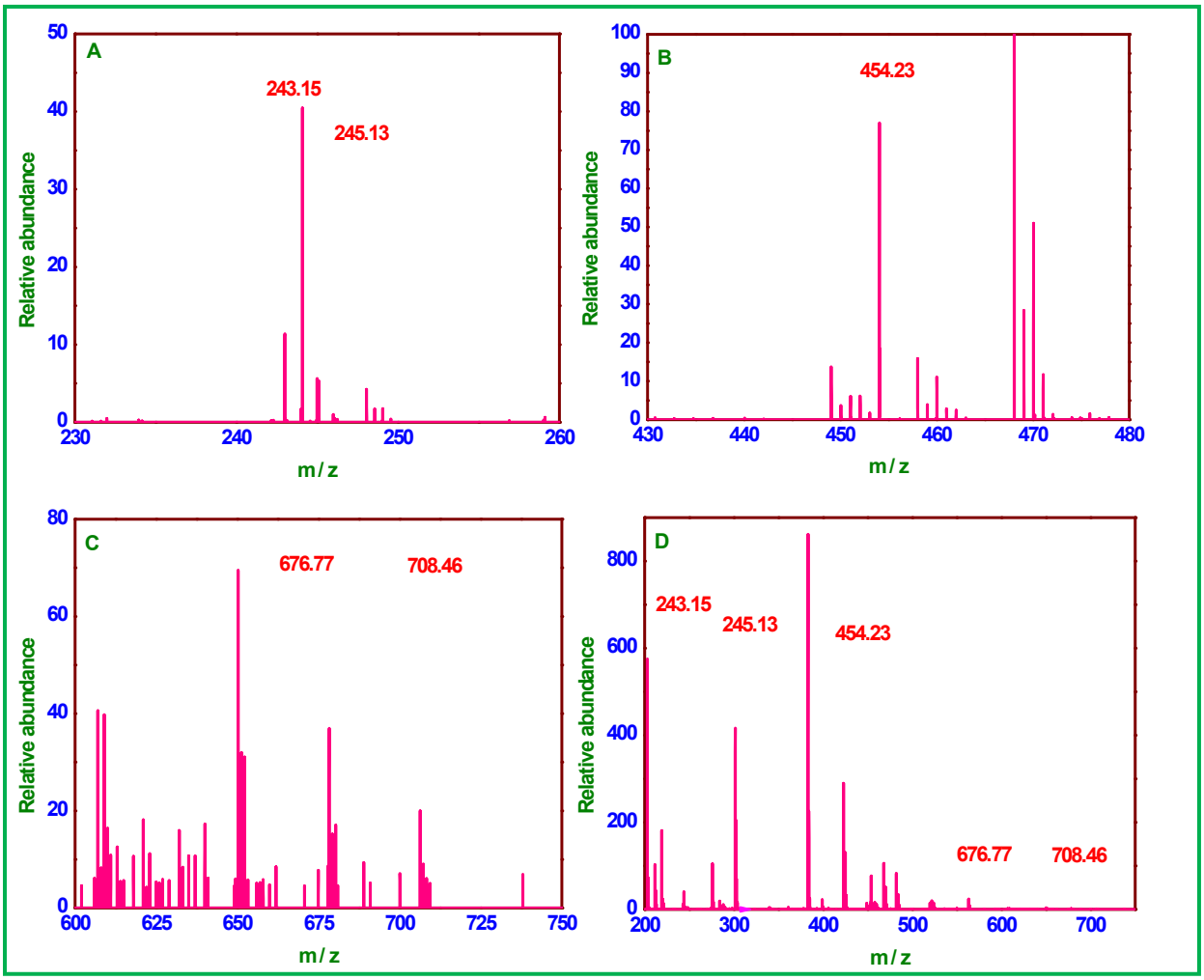

Fig. S52 HRMS spectra of a mixture containing [Cu(L^1)(phen)](ClO_4) (**1**) and H_2A (molar ratio, 1:50) after 10 minutes in buffer (pH 7.6) solution. (A) m/z 230-260, (B) m/z 430-480, (C) m/z 600- 750 and (D) full mass spectrum.

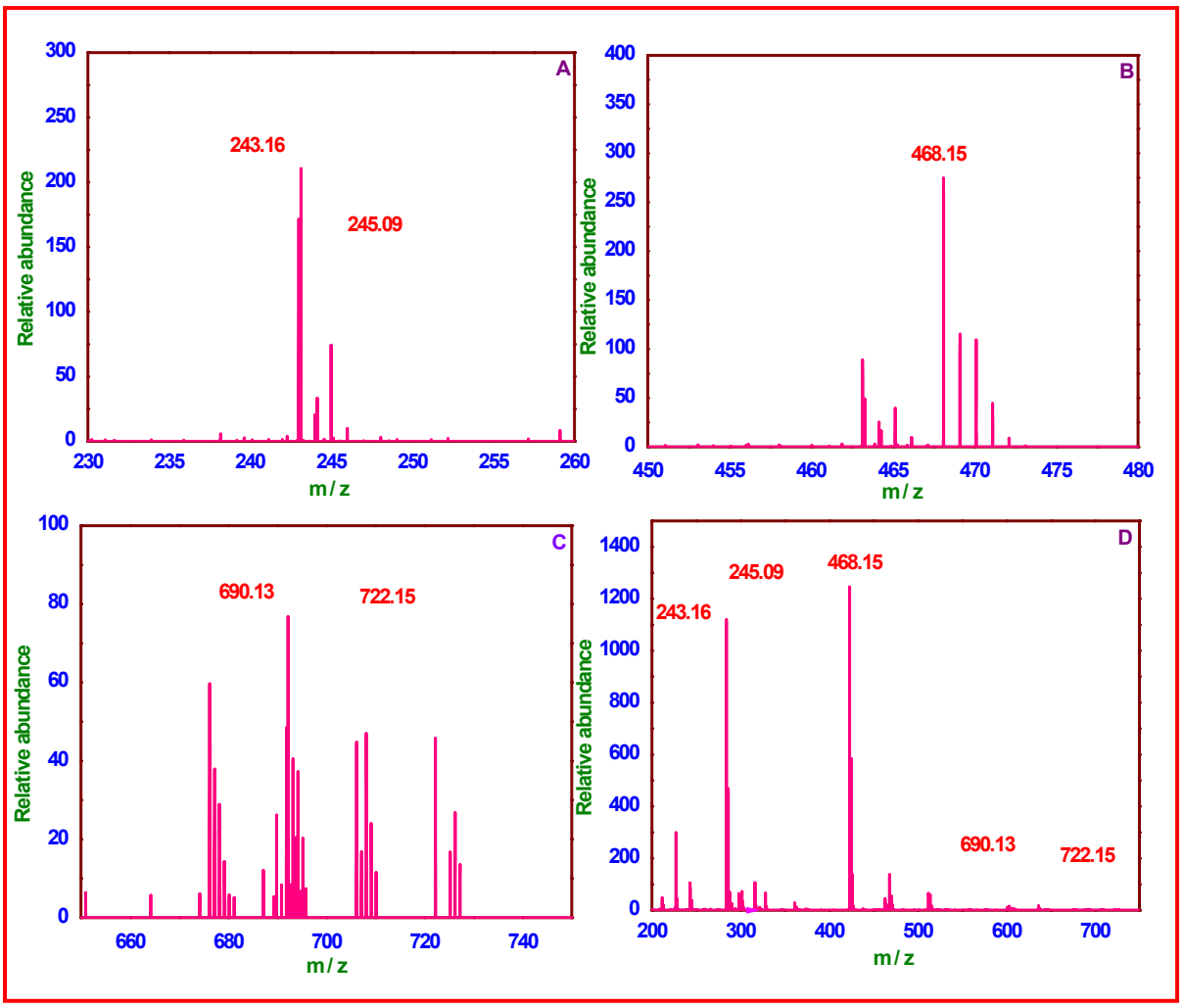

Fig. S53 HRMS spectra of a mixture containing [Cu(L^2)(phen)](ClO_4) (**2**) and 3,5-DTBC (molar ratio, 1:50) after 10 minutes in MeOH. (A) m/z 230-260, (B) m/z 450-480, (C) m/z 650-750 and (D) full mass spectrum.

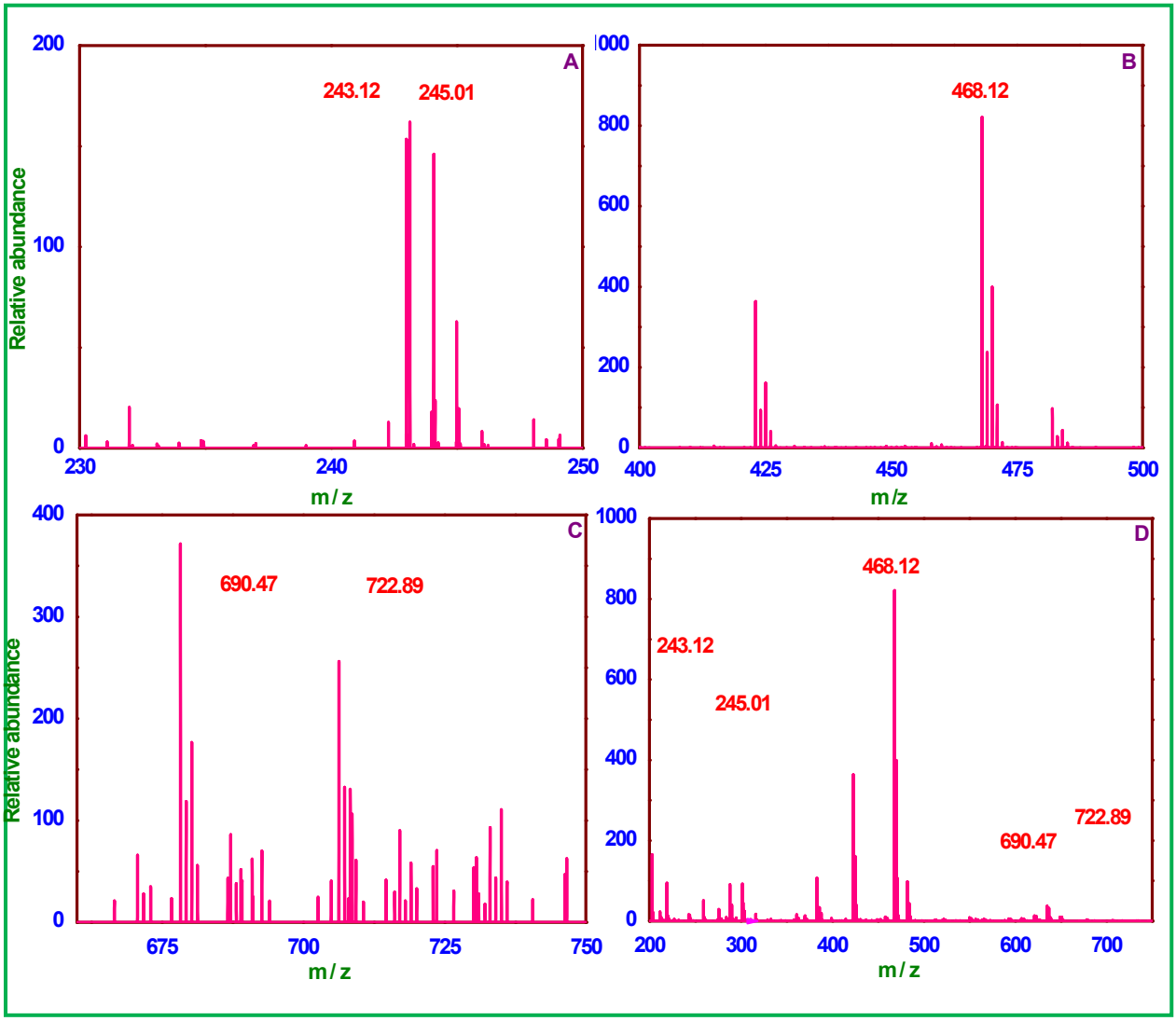

Fig. S54 HRMS spectra of a mixture containing [Cu(L^2)(phen)](ClO_4) (**2**) and 3,5-DTBC (molar ratio, 1:50) after 10 minutes in pH (7.8) solution. (A) m/z 230-260, (B) m/z 400-500, (C) m/z 650-750 and (D) full mass spectrum.

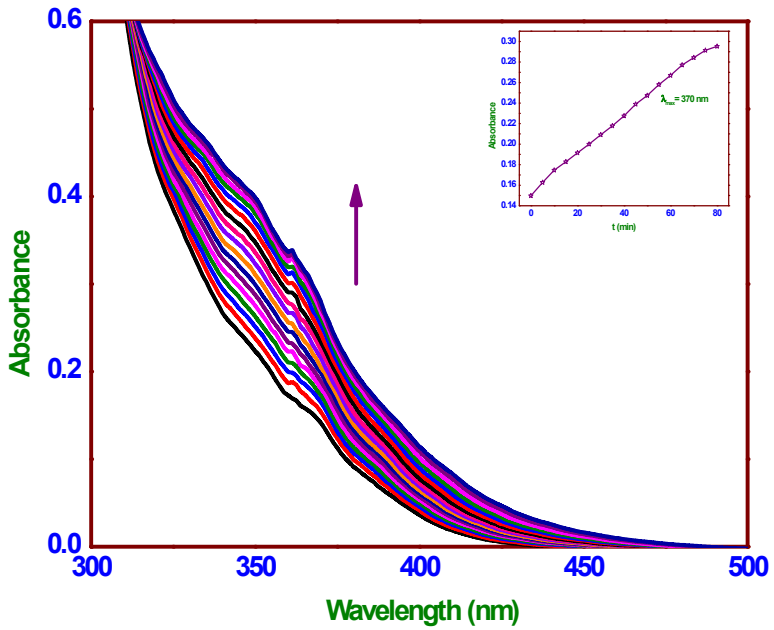

Fig. S55 UV-Visible spectroscopic monitoring of the reaction between [Cu(L^1)(phen)](ClO_4) (**1**) (2.9×10^{-5} M) and H_2O_2 (8.7×10^{-4} M) at room temperature in MeCN (molar ratio 1:30). Inset: Plot of Absorbance (370 nm) vs. time.

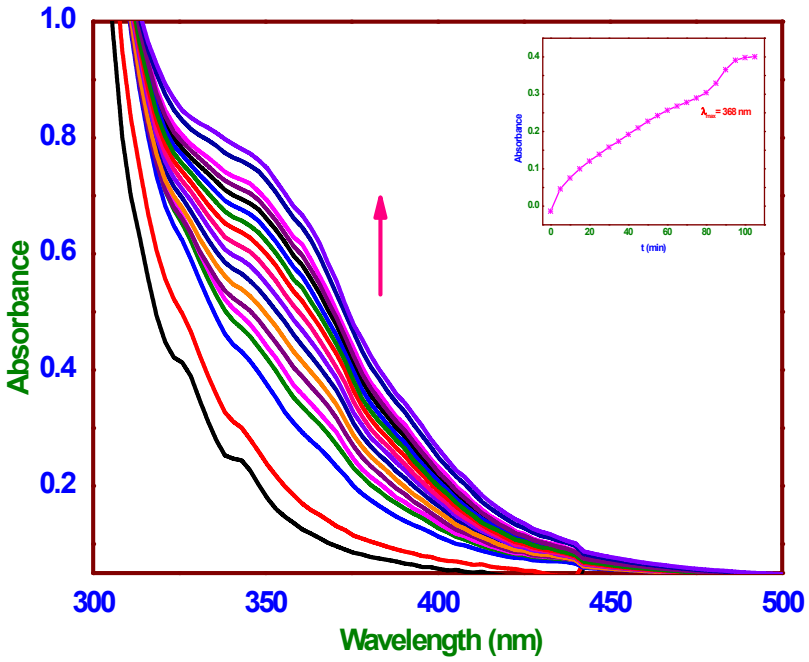

Fig. S56 UV-Visible spectroscopic monitoring of the reaction between [Cu(L^2)(phen)](ClO_4) (**2**) (2.9×10^{-5} M) and H_2O_2 (8.7×10^{-4} M) at room temperature in MeCN (molar ratio, 1:30). Inset: Plot of Absorbance (368 nm) vs. time.

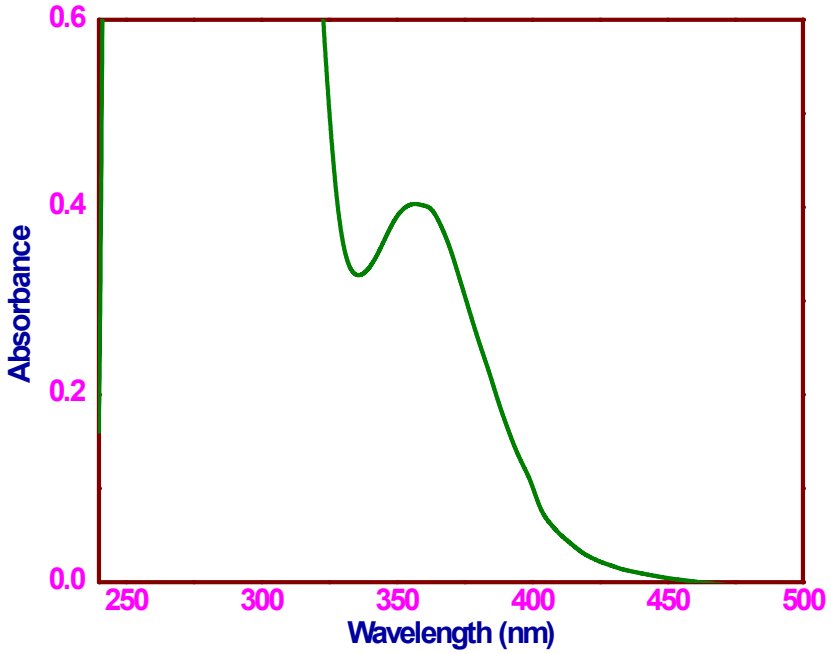

Fig. S57 Electronic spectrum of I_3^- obtained from the oxidation of I^- by H_2O_2 generated during catalytic cycle of 3,5-DTBC to 3,5-DTBQ.

References

1 M. J. Frisch, G. W. Trucks, H. B. Schlegel, G. E. Scuseria, M. A. Robb, J. R. Cheeseman, G. Scalmani, V. Barone, B. Mennucci, G. A. Petersson, H. Nakatsuji, M. Caricato, X. Li, H. P. Hratchian, A. F. Izmaylov, J. Bloino, G. Zheng, J. L. Sonnenberg, M. Hada, M. Ehara, K. Toyota, R. Fukuda, J. Hasegawa, M. Ishida, T. Nakajima, Y. Honda, O. Kitao, H. Nakai, T. Vreven, J. A. Montgomery, Jr., J. E. Peralta, F.Ogliaro, M. Bearpark, J. J. Heyd, E. Brothers, K. N. Kudin, V. N. Staroverov, R. Kobayashi, J. Normand, K. Raghavachari, A. Rendell, J. C. Burant, S. S. Iyengar, J. Tomasi, M. Cossi, N. Rega, J. M. Millam, M. Klene, J. E. Knox, J. B. Cross, V. Bakken, C. Adamo, J. Jaramillo, R. Gomperts, R. E. Stratmann, O. Yazyev, A. J. Austin, R. Cammi, C. Pomelli, J. W. Ochterski, R. L. Martin, K. Morokuma, V. G. Zakrzewski, G. A. Voth, P. Salvador, J. J. Dannenberg, S. Dapprich, A. D. Daniels, Ö. Farkas, J. B. Foresman, J. V. Ortiz, J. Cioslowski, D. J. Fox, Gaussian 09, Revision A.1, Gaussian, Inc., Wallingford CT, 2009.

2 (a) A. D. Becke, *J. Chem. Phys.* 1993, **98**, 1372-1377; (b) P. J. Hay, W. R. Wadt, *J. Chem. Phys*. 1985, **82**, 270-283; (c) P. J. Hay, W. R. Wadt, *J. Chem. Phys*. 1985, **82**, 299-310.

3 F. Weinhold, C. R. Landis, *Chem. Educ. Res. Pract.* 2001, **2**, 91-104.

4 J. D. Bradley, G. C. Gerrans, *J. Chem. Educ.* 1973, **50,** No. 463.

5 C.-G. Zhan, J. A. Nichols, D. A. Dixon, *J. Phys. Chem. A* 2003, **107**, 4184-4195.

6 W. T. Yang, R. G. Parr, *Proc. Natl. Acad. Sci. U.S.A.* 1985, **82**, 6723-6726.

7 M. Berkowitz, *J. Am. Chem. Soc.* 1987, **109**, 4823-4825.

8 S. B. Liu, *J. Chem. Sci.* 2005, ***117***, 477-483.